NATIONAL ADVISORY COMMITTEE FOR AERONAUTICS

TECHNICAL NOTE 2955

ESTIMATION OF FORCES AND MOMENTS DUE TO ROLLING FOR SEVERAL SLENDER-TAIL CONFIGURATIONS AT SUPERSONIC SPEEDS

By Percy J. Bobbitt and Frank S. Malvestuto, Jr.

Langley Aeronautical Laboratory
Langley Field, Va.

Washington
July 1953

NATIONAL ADVISORY COMMITTEE FOR AERC

TECHNICAL NOTE 2955

ESTIMATION OF FORCES AND MOMENTS DUE TO ROLLING FOR SEVERAL SLENDER-TAIL CONFIGURATIONS AT SUPERSONIC SPEEDS

By Percy J. Bobbitt and Frank S. Malvestuto, Jr.

SUMMARY

The velocity potentials, span loadings, and corresponding force and moment derivatives have been theoretically evaluated for a number of slender-tail arrangements performing a steady rolling motion at supersonic speeds.

The method of analysis is based upon an application of conformal-transformation techniques. The utilization of these techniques allows the simple determination of the complex potentials for various types of two-dimensional boundary-value problems.

In addition, two simple and often-used approximations to the rolling derivatives have been compared with the corresponding exact values determined by the method presented in this report.

In order to show the importance of wing-tail interference, the effect of the flow field behind a rolling wing on the tail characteristics has been illustrated for a simple wing-tail arrangement.

INTRODUCTION

A definite need has been indicated for additional information on the contribution of various tail configurations to the lateral dynamic stability of airplanes and missiles at supersonic speeds. This need is especially acute with regard to information on tails which have only one plane of symmetry. Inasmuch as tail arrangements, in general, may be classed as nonplanar systems, the problem of estimating theoretically the aerodynamic loading for a prescribed motion, such as rolling, may entail some difficulty, particularly if the panels comprising the tail are broad and have subsonic leading edges.

The difficulty of obtaining rigorous solutions for three-dimensional nonplanar systems led to the slender-body theory. This approach considerably simplifies the analysis of such systems by allowing the neglect of compressibility effects and, as shown in a number of papers (refs. 1 to 5), permits a solution to be obtained by an evaluation of the incompressible disturbance potential in crossflow planes, which are defined as planes normal to the direction of relative flow. The application of slender-body theory has led to many worth-while results for a number of practical wing, wing-body, and tail-body configurations composed of pointed low-aspect-ratio lifting surfaces and slender pointed bodies (refs. 1 to 6). The damping-in-roll derivative for a slender-cruciform arrangement has been evaluated by Ribner in reference 6 and Adams in reference 3. A velocity-potential solution reported by Westwater (ref. 7) is used in reference 6 to give the damping-in-roll solution for a slender configuration consisting of an arbitrary number of symmetrically placed triangular panels intersecting in a common chord.

The present paper has two purposes. The first purpose is to determine the rolling and yawing moments due to rolling for a number of practical slender-tail arrangements. These arrangements consist of triangular-plan-form panels which intersect in a common chord but are not necessarily symmetrical with respect to this chord. The second purpose is to present the method used in solving the problem of the rolling two-dimensional boundary that was reported by Bickley in reference 8. This method, in which the conformal-transformation technique is used, allows the solution of a wide range of two-dimensional problems and is especially applicable when the contours of the tail arrangements in the crossflow planes are not symmetrical. Also included herein are the necessary transformations and the integral form of the potential for a tail arrangement consisting of slender triangular fins attached symmetrically to a slender circular cylinder.

In order to assess properly the contribution of the tail to the rolling and yawing moments due to rolling for a complete configuration, the effect of the induced flow behind a rolling triangular wing on the contribution of the tail is approximately determined.

For the reader whose primary interest is in the results rather than in the method, illustrative variations of the rolling stability derivatives for several series of tail arrangements, as well as sample span loadings and pressure distributions, are included in the figures. The formulas from which these loadings and derivatives have been obtained are presented in the section devoted to applications.

The greater part of this investigation was carried out early in 1952.

SYMBOLS

The positive directions of the forces, moments, and velocities are shown in figure 1.

x,y,z	Cartesian coordinates (original space coordinates)
Z	complex variable, $z + iy$
ζ	complex variable, $\xi + i\eta$
ξ,η	coordinates in complex ζ-plane
y_2'	spanwise variable in plane of wing
y_2	nondimensional spanwise variable in plane of wing, $\frac{y_2'}{b/2}$
y_1,z_1	nondimensional coordinates, $y_1 = \frac{y}{b/2}$, $z_1 = \frac{z}{b/2}$
u,v,w	perturbation velocity components in x-, y-, and z-directions, respectively
r	magnitude of vector in Z-plane
ρ	air density
V	flight velocity
Δp	local pressure difference across surface
q	free-stream dynamic pressure, $\frac{1}{2}\rho V^2$
$\Delta p/q$	pressure coefficient
M	free-stream Mach number
ϕ	perturbation velocity potential
ψ	stream function
W	complex potential, $\phi + i\psi$
β	angle of sideslip

p rate of roll, radians/sec

R ratio of span of vertical panel to span of horizontal tail for inverted T-tail

a function of R, $\left(\frac{1 + \sqrt{1 + 4R^2}}{2R^2}\right)^{1/2} = \left(\frac{1 + \cos \theta_1}{1 - \cos \theta_1}\right)^{1/2}$

K ratio of span of vertical tail to span of horizontal tail for cruciform tail

e function of K, $(K^2 + 1)^{1/2} - K = \left(\frac{1 + \cos \theta_1}{1 - \cos \theta_1}\right)^{1/2}$

c_r root chord

s spanwise variable along an arbitrary panel

s_o span of an arbitrary panel

h span of upper vertical panel

h_1 span of lower vertical panel

b span of horizontal tail

H, H_1, B dimensions of general cruciform tail obtained by transformation

l arbitrary length

S arbitrary area

A aspect ratio of horizontal tail, $\frac{b^2}{\text{Horizontal-tail area}}$

A_V aspect ratio of vertical tail, $\frac{(\text{Vertical-tail span})^2}{\text{Vertical-tail area}}$

$$A' = \frac{(\text{Twice span of largest panel})^2}{\text{Twice area of largest panel}}$$

r_o	body radius
Γ	spanwise circulation
δ_1	angle between root chord and leading edge of vertical panel
δ_2	angle between root chord and leading edge of horizontal panel
θ_1,θ_2	angles used in transformation of general cruciform from Z-plane to ζ-plane
τ	angle that panel makes with x,y plane
N'	normal force
Y	lateral force
L'	rolling moment about x-axis
N	yawing moment about z-axis
C_N	normal-force coefficient
C_l	rolling-moment coefficient, L'/qSl

$$(C_l)_{CT} = \frac{L'}{qb(\text{Horizontal-tail area})}$$

$$(C_l)_{TT} = \frac{L'}{qb(\text{Horizontal-tail area})}$$

$$(C_l)_{VT} = \frac{L'}{q(\text{Twice area of one panel})(\text{Twice span of one panel})}$$

$$(C_l)_{YT} = \frac{L'}{q(\text{Twice area of largest panel})(\text{Twice span of largest panel})}$$

$$C_{l_p} = \left(\frac{\partial C_l}{\partial \frac{pl}{2V}}\right)_{p \to 0}$$

$$\left(C_{l_p}\right)_{CT} = \left[\frac{\partial\left(C_l\right)_{CT}}{\partial\frac{pb}{2V}}\right]_{p\rightarrow 0}$$

$$\left(C_{l_p}\right)_{TT} = \left[\frac{\partial\left(C_l\right)_{TT}}{\partial\frac{pb}{2V}}\right]_{p\rightarrow 0}$$

$$\left(C_{l_p}\right)_{VT} = \left[\frac{\partial\left(C_l\right)_{VT}}{\partial\frac{p}{V}(\text{Span of one panel})}\right]_{p\rightarrow 0}$$

$$\left(C_{l_p}\right)_{YT} = \left[\frac{\partial\left(C_l\right)_{YT}}{\partial\frac{p}{V}(\text{Span of largest panel})}\right]_{p\rightarrow 0}$$

C_Y lateral-force coefficient, Y/qS

$$\left(C_Y\right)_{CT} = \frac{Y}{q(\text{Vertical-tail area})}$$

$$\left(C_Y\right)_{TT} = \frac{Y}{q(\text{Vertical-panel area})}$$

$$\left(C_Y\right)_{VT} = \frac{Y}{2q(\text{Area of one panel})}$$

$$\left(C_Y\right)_{YT} = \frac{Y}{2q(\text{Area of largest panel})}$$

$$C_{Y_p} = \left(\frac{\partial C_Y}{\partial \frac{pl}{2V}} \right)_{p \to 0}$$

$$(C_{Y_p})_{CT} = \left[\frac{\partial (C_Y)_{CT}}{\partial \frac{p}{V} \frac{\text{(Vertical-tail span)}}{2}} \right]_{p \to 0}$$

$$(C_{Y_p})_{TT} = \left[\frac{\partial (C_Y)_{TT}}{\partial \frac{p}{V} \text{(Vertical-panel span)}} \right]_{p \to 0}$$

$$(C_{Y_p})_{VT} = \left[\frac{\partial (C_Y)_{VT}}{\partial \frac{p}{V} \text{(Span of one panel)}} \right]_{p \to 0}$$

$$(C_{Y_p})_{YT} = \left[\frac{\partial (C_Y)_{YT}}{\partial \frac{p}{V} \text{(Span of largest panel)}} \right]_{p \to 0}$$

C_n yawing-moment coefficient, N/qSl

$$C_{n_p} = \left(\frac{\partial C_n}{\partial \frac{pl}{2V}} \right)_{p \to 0}$$

$$(C_{l_\beta})_{TT} = \left[\frac{\partial (C_l)_{TT}}{\partial \beta} \right]_{\beta \to 0}$$

$$C_{Y_\beta} = \left(\frac{\partial C_Y}{\partial \beta}\right)_{\beta \to 0}$$

$$\left(C_{Y_\beta}\right)_{TT} = \left[\frac{\partial \left(C_Y\right)_{TT}}{\partial \beta}\right]_{\beta \to 0}$$

Subscripts:

TE	trailing edge
LE	leading edge
CT	cruciform tail
TT	inverted T-tail
VT	V-tail
YT	Y-tail
z,y	real and imaginary parts of a function, respectively

GENERAL ANALYSIS

Linearized three-dimensional supersonic flow is governed by the classical partial-differential equation

$$(M^2 - 1)\phi_{xx} - \phi_{yy} - \phi_{zz} = 0 \qquad (1)$$

where ϕ is the disturbance velocity potential. If the disturbance body is slender in the axial direction, the potential flow is, to a satisfactory approximation (see refs. 4 and 9), controlled by the two-dimensional Laplace equation

$$\phi_{yy} + \phi_{zz} = 0 \qquad (2)$$

Briefly, the classification of a body as slender means that the production of perturbated flow in any cross plane (y,z plane) normal

to the free-stream direction (x-axis) is dependent only upon the disturbance contour in that plane and, hence, independent of the flow action in the preceding cross planes. Such a consideration implies the neglect of the gradient of flow in the longitudinal direction and necessitates the removal of the $(M^2 - 1)\phi_{xx}$ term from equation (1). It seems reasonable to expect that the application of slender-body theory should give with satisfactory accuracy the aerodynamic loading for slender configurations for which the boundary conditions (such as rolling) do not depend explicitly on the longitudinal distance.

Boundary Conditions

Sketches of the tail arrangements considered in this paper are presented in figure 1. Figure 2 presents a cross-sectional view of these arrangements and the prescribed boundary conditions for steady rolling motion. In the crossflow planes represented in figure 2, the two-dimensional potential flow satisfies the Laplace equation (eq. (2)), and the perturbated v and w velocities external to the disturbance contours must be continuous except possibly at the edges of the contour. As infinity is approached, the potential and the v and w velocities must become zero. Across the contour the normal flow velocity is continuous; whereas, the tangential flow velocity is discontinuous.

Determination of Velocity-Potential Function

The determination of the velocity potential in the crossflow planes for the tail arrangements shown in figure 2 can be simplified by a conformal transformation of the regions external to the disturbance contours to an upper half plane, the closed disturbance contours being transformed into the infinite real axis of the transformed plane. The velocity potential is then readily obtained in this plane, and by an inverse of the transformation, the expression for the velocity potential is established in the original plane. A brief discussion of the required conformal-transformation theory with particular emphasis on a rotating boundary (such as a rolling tail) is presented in the following section.

Conformal transformations and auxiliary functions.- Any one of the crossflow planes for the tail configurations shown in figure 2 is called the original plane and designated symbolically as the Z-plane. The ζ-plane ($\zeta = \xi + i\eta$) is designated as the complex plane in which the real axis is the transformed contour of the original plane and the upper half plane is the transformed region exterior to the contour in the original plane.

As is well-known, the transformation of an arbitrary, closed, rectilinear polygon from the Z-plane into the upper half of the ζ-plane can be expressed by the following form of the Schwarz-Christoffel transformation:

$$\frac{dZ}{d\zeta} = \frac{(\text{Complex constant})\Pi(\zeta - c)^{\gamma/\pi}}{(\zeta^2 + 1)^2} \tag{3}$$

where the position of the pole has been taken at $\zeta = i$. The symbol γ denotes the exterior angles of the polygon and c denotes the points in the ζ-plane which correspond to the vertices of the polygon in the Z-plane. The symbol Π denotes the fact that each corner of the polygon requires a factor $(\zeta - c)^{\gamma/\pi}$ in the formula for $dZ/d\zeta$. The use of this expression requires that the numerator have no zeros and no branch points in the upper half of the ζ-plane and, consequently, none in the lower half plane. Integration of equation (3) yields

$$Z = \frac{g(\zeta)}{\zeta^2 + 1} \tag{4}$$

where $g(\zeta)$ is specified by the following relationship:

$$(\text{Complex constant})\Pi(\zeta - c)^{\gamma/\pi} = g'(\zeta)(\zeta^2 + 1) - 2\zeta g(\zeta)$$

The determination of the $g(\zeta)$ function may be very difficult for some configurations. This transformation procedure is illustrated in reference 8.

For convenience, the points defining the boundary contour in the Z-plane are denoted by $z + iy$; hence, the conformal relation between the original and transformed boundary becomes

$$Z = z + iy = \frac{g(\xi)}{\xi^2 + 1} \tag{5}$$

where ξ represents points along the real axis (the transformed boundary) in the ζ-plane. The preceding transformation may be expressed as

$$Z = \frac{g_z(\xi) + ig_y(\xi)}{\xi^2 + 1} \tag{6}$$

or

$$z = \frac{g_z(\xi)}{\xi^2 + 1} \qquad y = \frac{g_y(\xi)}{\xi^2 + 1}$$

Note that $g_z(\xi)$ and $g_y(\xi)$ are real-valued functions of ξ.

The following relationships are extremely helpful in the transformation of the boundary conditions from the contour in the Z-plane to the transformed contour (the real axis) in the ζ-plane, particularly when the contour in the original plane is experiencing a steady rolling motion. On the boundary in the Z-plane, $Z\overline{Z} = |Z|^2 = r^2$ where r is the magnitude of the vector-point function from the origin to the boundary. In the ζ-plane, the relation $Z\overline{Z} = r^2$ transforms into $\frac{h(\xi)}{(\xi^2 + 1)^2}$ where $h(\xi)$ is defined as

$$h(\xi) = \left[g_z(\xi)\right]^2 + \left[g_y(\xi)\right]^2 \tag{7}$$

On the boundary $\overline{Z} = \frac{\overline{g(\zeta)}}{\zeta^2 + 1}$; hence, from this relation and equation (4)

$$Z\overline{Z} = r^2 = \frac{g(\zeta)\overline{g(\zeta)}}{(\zeta^2 + 1)^2} \tag{8}$$

(It should be noted that eq. (8) applies only on the boundary.)

and

$$h(\zeta) = g(\zeta)\overline{g(\bar{\zeta})} = \left[g_z(\zeta)\right]^2 + \left[g_y(\zeta)\right]^2 \tag{9}$$

which are the useful and necessary expressions that relate the original and transformed boundary conditions in the Z- and ζ-planes, respectively. Points on the boundary in the Z-plane coincident with the z or the y coordinate axis will take on values in the ζ-plane given by either $\left[g_z(\xi)\right]^2$ or $\left[g_y(\xi)\right]^2$.

As an illustration of the use of the preceding relationships, consider the following example: Given a boundary in the Z-plane which is rolling with steady angular velocity p about an axis through the origin of the boundary and normal to the plane of the boundary. The distribution of the prescribed normal velocity along the boundary is equal to pr, and this distribution must be equal to the tangential derivative of the stream function along the boundary. Hence, if the complex potential function is $W = \phi + i\psi$, then $\frac{1}{2}pr^2 = \psi$ along the boundary. Now $r^2 = |Z|^2$ and, from the preceding discussion, the boundary condition for rolling in the Z-plane $\frac{1}{2}p|Z|^2$ transforms by use of equations (8) and (9) into $\frac{1}{2}p\,\frac{h(\xi)}{(\xi^2 + 1)^2}$ along the transformed boundary (which is the infinite real axis) in the ζ-plane.

Integral expression for the potential in the ζ-plane.- As indicated in the previous section, the contour in the original plane is transformed into the real axis of the ζ-plane, and the region external to the contour is transformed into the upper half of the ζ-plane. In this plane the complex velocity potential $W(\zeta) = \phi(\zeta) + i\psi(\zeta)$ is determined so that it satisfies the prescribed distribution of normal velocity along the boundary of the real axis. This normal velocity distribution, as shown previously, manifests itself through the stream function $\psi(\xi)$ along the boundary. The remaining problem is to determine a function of ζ that is finite and single-valued in the upper half of the ζ-plane with the imaginary part tending to $\psi(\xi)$ as ζ approaches the boundary of the real axis from above. Bickley (ref. 8) presents the following integral function of ζ which satisfies these requirements:

$$W(\zeta) = \frac{1}{\pi}\int_{-\infty}^{\infty} \frac{\psi(\xi)d\xi}{\xi - \zeta} \tag{10}$$

In the appendix this integral solution presented by Bickley is shown to be a special case of the general solution of the Riemann-Hilbert problem for the half plane which is reported by Muskhelishvili (ref. 10). For the case of the rotating boundary, $\psi(\xi)$ becomes $\frac{ph(\xi)}{2(\xi^2 + 1)^2}$ as previously noted. The following integral expression is then obtained as the complex potential in the ζ-plane for the case of a rotating boundary in the original plane (see ref. 8):

$$W(\zeta) = \frac{p}{2\pi}\int_{-\infty}^{\infty} \frac{h(\xi)}{(\xi^2 + 1)^2}\frac{d\xi}{(\xi - \zeta)} \tag{11}$$

Expressions for Pressures, Forces, and Moments

Once the velocity potential has been determined subject to the required boundary conditions, the expressions for the lifting pressure and the corresponding forces and moments are easily obtained. The lifting-pressure coefficient is given by

$$\frac{\Delta p}{q} = \frac{2}{V}\frac{\partial \Delta\phi}{\partial x} = \frac{2}{V}\frac{\partial \Delta\phi}{\partial s_o}\frac{\partial s_o}{\partial x} = \frac{2}{V}\frac{\partial \Gamma}{\partial s_o}\frac{\partial s_o}{\partial x} \tag{12}$$

where Γ, the spanwise circulation, is defined as $\phi_1 - \phi_2$, the potential jump across the surface. The subscripts simply denote values on opposite sides of a surface. Equation (12) is consistent with the small-perturbation theory only if the magnitudes of the perturbation velocities are equal across the lifting surface. When the magnitudes of the perturbation velocities are not equal across the lifting surface, equation (12) should contain differences in the squares of the v and w velocities. The squared terms contribute terms which are linear functions of p to the stability derivatives; therefore, these terms will vanish because the derivatives are to be evaluated as $p \longrightarrow 0$.

The expression for the normal force acting on a panel of the tail configuration is

$$N' = \rho V \int_0^{s_o}\int_{L.E.}^{T.E.} \frac{\partial \Gamma}{\partial x}\, ds\, dx \tag{13}$$

or, since $\Gamma_{LE} = 0$,

$$N' = \rho V \int_0^{s_o} \Gamma_{TE}\, ds \tag{14}$$

Reduction to coefficient form by dividing by qS yields

$$C_N = \frac{2}{VS} \int_0^{s_o} \Gamma_{TE}\, ds \tag{15}$$

The integral expression for the moment of the normal force is readily obtained on the basis of previously published analyses which have shown that, for rolling triangular arrangements with pressure coefficients of the form $ps_o f(s/s_o)$, the longitudinal location of the center of pressure is at the $\frac{3}{4}c_r$ point. With this stipulation, the yawing moment about the apex of the tail system may be expressed as

$$N = \frac{3}{4} c_r \rho V \sin \tau \int_0^{s_o} \Gamma_{TE}\, ds \tag{16}$$

and division by qSl gives

$$C_n = \frac{3}{2} c_r \frac{\sin \tau}{VSl} \int_0^{s_o} \Gamma_{TE}\, ds \tag{17}$$

The rolling moment about the longitudinal axis is given by

$$L' = \rho V \int_0^{s_o} \Gamma_{TE} s\, ds \tag{18}$$

and nondimensionally by

$$C_{l_p} = \frac{4}{pSl^2} \int_0^{s_o} \Gamma_{TE} s\, ds \tag{19}$$

For certain configurations it may be expedient, in order to facilitate integration operations, to determine the rolling and yawing moments by a consideration of the potential expression in the ζ-plane instead of the original Z-plane. The necessary expressions for the moments are easily derived as follows: The rolling moment in the original plane can be expressed as

$$L' = \rho V \oint \phi_{TE}(z\, dz + y\, dy)$$

or

$$L' = \rho V \oint \phi_{TE}\, d\left(\frac{1}{2} r^2\right)$$

Integration by parts gives

$$L' = \frac{1}{2} \rho V \phi_{TE} r^2 - \frac{1}{2} \rho V \oint r^2 d\phi_{TE} \tag{20a}$$

In the ζ-plane equation (20a) may be expressed as

$$L' = \frac{1}{2} \rho V \int_{-\infty}^{\infty} \frac{h(\xi)}{(\xi^2 + 1)^2} \frac{d\phi}{d\xi}\, d\xi \tag{20b}$$

when the contour in the original plane is assumed to be symmetrical, at least with respect to one of the coordinate axes. This condition of symmetry, together with the antisymmetrical nature of the potential, causes the disappearance of the first term on the right-hand side of equation (20a) which expresses the rolling moment in the Z-plane. Similarly, the moment of the normal force (referred to the apex) may also be more easily obtained if the integration is performed in the ζ-plane as follows:

$$N = \frac{3}{4} c_r \sin \tau\, \rho V \left(\int_{a'}^{b'} \phi \frac{ds}{d\xi}\, d\xi - \int_{c'}^{d'} \phi \frac{ds}{d\xi}\, d\xi \right) \tag{21}$$

where $a'b'$ and $c'd'$ are those portions of the ξ-axis corresponding to opposite sides of a panel in the original plane. The side force, of course, is simply N divided by $\frac{3}{4} c_r$.

APPLICATIONS

The results of the preceding analysis are applied in this section to the evaluation of the velocity potentials and associated force and moment derivatives for several tail arrangements. In addition, a brief discussion of the effect of the wing flow field on the tail characteristics is included.

Forces and Moments on Rolling Tails

General cruciform tail arrangement (symmetrical with respect to one plane).- The transformation of the space outside a cruciform with vertical panels of different spans and horizontal panels of equal spans to the upper half of the ζ-plane is obtained from reference 11 as

$$Z = \pm \frac{2\left[\zeta^4(1 - \cos\theta_1)(1 - \cos\theta_2) + 2\zeta^2(\cos\theta_1 \cos\theta_2 - 1) + (1 + \cos\theta_1)(1 + \cos\theta_2)\right]^{1/2}}{\zeta^2 + 1} \tag{22}$$

The orientation of the cruciform in the Z-plane and the correspondence of points in the Z- and ζ-planes may be noted from figure 3. The dimensions of the cruciform tail (that is, the panel spans H, H_1, and $B/2$), as transformed by equation (22), are determined by the selection of $\cos\theta_1$ and $\cos\theta_2$ in the following equations (ref. 11):

$$H = 2\left[(1 - \cos\theta_1)(1 - \cos\theta_2)\right]^{1/2} \tag{23a}$$

$$H_1 = 2\left[(1 + \cos\theta_1)(1 + \cos\theta_2)\right]^{1/2} \tag{23b}$$

$$\frac{B}{2} = \cos\theta_1 - \cos\theta_2 \tag{23c}$$

In order to facilitate the selection of the cosine terms for known ratios of H/H_1 and $\frac{B/2}{H_1}$, equations (23) may be written in the following form:

$$\left.\begin{aligned}
\cos\theta_1 = {} & \frac{\left(\frac{H}{H_1}\right)^2 + 1 + 2\,\frac{B/2}{H_1}\left(\frac{H}{H_1}\right)^2\left[\frac{B/2}{H_1} + \sqrt{\left(\frac{B/2}{H_1}\right)^2 + 1}\right]}{2\,\frac{B/2}{H_1}\left[\left(\frac{H}{H_1}\right)^2 - 1\right]\left[\frac{B/2}{H_1} + \sqrt{\left(\frac{B/2}{H_1}\right)^2 + 1}\right] + \left(\frac{H}{H_1}\right)^2 - 1} - \\
& \frac{2\sqrt{\left\{\frac{B/2}{H_1}\left[\frac{B/2}{H_1} + \sqrt{\left(\frac{B/2}{H_1}\right)^2 + 1}\right] + \left(\frac{H}{H_1}\right)^2\right\}^2 - \left(\frac{H}{H_1}\right)^2\left[\left(\frac{H}{H_1}\right)^2 - 1\right]}}{2\,\frac{B/2}{H_1}\left[\left(\frac{H}{H_1}\right)^2 - 1\right]\left[\frac{B/2}{H_1} + \sqrt{\left(\frac{B/2}{H_1}\right)^2 + 1}\right] + \left(\frac{H}{H_1}\right)^2 - 1} \\
\cos\theta_2 = {} & \frac{\left(\frac{H}{H_1}\right)^2 + 1 + 2\,\frac{B/2}{H_1}\left(\frac{H}{H_1}\right)^2\left[\frac{B/2}{H_1} - \sqrt{\left(\frac{B/2}{H_1}\right)^2 + 1}\right]}{2\,\frac{B/2}{H_1}\left[\left(\frac{H}{H_1}\right)^2 - 1\right]\left[\frac{B/2}{H_1} - \sqrt{\left(\frac{B/2}{H_1}\right)^2 + 1}\right] + \left(\frac{H}{H_1}\right)^2 - 1} - \\
& \frac{2\sqrt{\left\{\frac{B/2}{H_1}\left[\frac{B/2}{H_1} - \sqrt{\left(\frac{B/2}{H_1}\right)^2 + 1}\right] + \left(\frac{H}{H_1}\right)^2\right\}^2 - \left(\frac{H}{H_1}\right)^2\left[\left(\frac{H}{H_1}\right)^2 - 1\right]}}{2\,\frac{B/2}{H_1}\left[\left(\frac{H}{H_1}\right)^2 - 1\right]\left[\frac{B/2}{H_1} - \sqrt{\left(\frac{B/2}{H_1}\right)^2 + 1}\right] + \left(\frac{H}{H_1}\right)^2 - 1}
\end{aligned}\right\} \tag{24}$$

It is evident from the transformation that Z will be either real or imaginary on the boundary. The auxiliary function $h(\xi)$ will therefore be given by

$$h(\xi) = \pm 4\left[\xi^4(1 - \cos\theta_1)(1 - \cos\theta_2) + 2\xi^2(\cos\theta_1 \cos\theta_2 - 1) + (1 + \cos\theta_1)(1 + \cos\theta_2)\right] \tag{25}$$

where the negative sign applies over the portions of the boundary from the points ⑧ to ⑥ and ④ to ② (see fig. 3(c)) and the positive sign applies over the remaining portions of the boundary. Substituting these $h(\xi)$ functions into equation (11) and performing the indicated integration results in the following expression for the complex potential in the ζ-plane:

$$W = \frac{4p}{\pi}\left\{2\left[\frac{2\zeta(F_1 - F_2 - 1)}{\zeta^2 + 1} - \frac{4\zeta}{(\zeta^2 + 1)^2}\right]\left(\tan^{-1}\sqrt{F_3 - F_4} - \tan^{-1}\sqrt{F_3 + F_4} + \frac{\pi}{4}\right) + \frac{4\zeta}{\zeta^2 + 1}\left(\frac{\sqrt{F_3 + F_4}}{F_3 + F_4 + 1} - \frac{\sqrt{F_3 - F_4}}{F_3 - F_4 + 1}\right) + \left[\frac{F_1\zeta^4 + 2F_2\zeta^2 + 4 + 2F_2 - F_1}{(\zeta^2 + 1)^2}\right]\left[\log_e \frac{\left(\sqrt{F_3 + F_4} + \zeta\right)\left(\sqrt{F_3 - F_4} - \zeta\right)}{\left(\sqrt{F_3 - F_4} + \zeta\right)\left(\sqrt{F_3 + F_4} - \zeta\right)} + i\frac{\pi}{2}\right]\right\} \tag{26}$$

where

$$F_1 = (1 - \cos\theta_1)(1 - \cos\theta_2)$$

$$F_2 = \cos\theta_1 \cos\theta_2 - 1$$

$$F_3 = \frac{1 - \cos\theta_1 \cos\theta_2}{(1 - \cos\theta_1)(1 - \cos\theta_2)}$$

$$F_4 = \frac{\cos\theta_1 - \cos\theta_2}{(1 - \cos\theta_1)(1 - \cos\theta_2)}$$

If, in equation (26), ζ is expressed in terms of Z (obtained from eq. (22)), there results the complex potential in the original plane (the Z-plane) for a cruciform with the dimensions H, H_1, and $B/2$ (see eqs. 23).

The velocity potential in the ζ-plane (real part of eq. (26)), together with the $h(\xi)$ functions (eq. (25)) and the relation in equation (20b), yields the rolling moment and, hence, the damping-in-roll coefficient as

$$\left(C_{l_p}\right)_{CT} = \frac{-4A}{\pi(F_1F_4)^4}\left[-8\left[\pi - 4\left(\tan^{-1}\sqrt{F_3 + F_4} - \tan^{-1}\sqrt{F_3 - F_4}\right)\right]\left[\frac{\sqrt{F_3 + F_4}}{(1 + F_3 + F_4)^4} - \frac{\sqrt{F_3 - F_4}}{(1 + F_3 - F_4)^4}\right] + \right.$$

$$\left\{\left[\pi - 4\left(\tan^{-1}\sqrt{F_3 + F_4} - \tan^{-1}\sqrt{F_3 - F_4}\right)\right]\left[8(F_1 - F_2) - 4\right] + 16\left(\frac{\sqrt{F_3 + F_4}}{1 + F_3 + F_4} - \right.\right.$$

(Equation continued on next page)

$$\frac{\sqrt{F_3 - F_4}}{1 + F_3 - F_4}\Bigg)\Bigg\}\left[\frac{\sqrt{F_3 + F_4}}{(1 + F_3 + F_4)^3} - \frac{\sqrt{F_3 - F_4}}{(1 + F_3 - F_4)^3}\right] + \Bigg\{\Big(\pi - 4\tan^{-1}\sqrt{F_3 + F_4} -$$

$$\tan^{-1}\sqrt{F_3 - F_4}\Big)\left(-4F_2 - 3 - 2F_2^2 + 4F_1F_2 - 2F_1^2\right) + \frac{\sqrt{F_3 + F_4}}{1 + F_3 + F_4}\left[\frac{8}{1 + F_3 + F_4} +\right.$$

$$\left.16(F_2 - F_1) + 12\right] - \frac{\sqrt{F_3 - F_4}}{1 + F_3 - F_4}\left[\frac{8}{1 + F_3 - F_4} + 16(F_2 - F_1) + 12\right]\Bigg\}\left[\frac{\sqrt{F_3 + F_4}}{(1 + F_3 + F_4)^2} -\right.$$

$$\left.\frac{\sqrt{F_3 - F_4}}{(1 + F_3 - F_4)^2}\right] + \Bigg\{\left[\pi - 4\left(\tan^{-1}\sqrt{F_3 + F_4} - \tan^{-1}\sqrt{F_3 - F_4}\right)\right]\frac{-9 - 8F_2 + 4F_1 + 2F_1^2 - 2F_2^2}{2} +$$

$$\frac{\sqrt{F_3 + F_4}}{1 + F_3 + F_4}\left[\frac{16}{(1 + F_3 + F_4)^2} + \frac{16(F_2 - F_1) + 12}{1 + F_3 + F_4} + 4F_2^2 - 8F_1F_2 + 4F_1^2 + 16F_2 + 18\right] -$$

(Equation continued on next page)

$$\frac{\sqrt{F_3 - F_4}}{1 + F_3 - F_4}\left[\frac{16}{(1 + F_3 - F_4)^2} + \frac{16(F_2 - F_1) + 12}{1 + F_3 - F_4} + 4F_2^2 - 8F_1F_2 + 4F_1^2 + 16F_2 + 18\right]\left(\frac{\sqrt{F_3 + F_4}}{1 + F_3 + F_4} - \frac{\sqrt{F_3 - F_4}}{1 + F_3 - F_4}\right) - \left(\left[\pi - 4\left(\tan^{-1}\sqrt{F_3 + F_4} - \tan^{-1}\sqrt{F_3 - F_4}\right)\right]\frac{-2F_1^2 + 4F_1F_2 + 8F_1 - 2F_2^2 - 8F_2 - 9}{2} + \frac{\sqrt{F_3 + F_4}}{1 + F_3 + F_4}\left\{\frac{32}{(1 + F_3 + F_4)^3} + \frac{32(F_2 - F_1) + 16}{(1 + F_3 + F_4)^2} + \frac{8\left[(F_2 - F_1)^2 + 2F_1\right] + 16(F_2 - F_1) + 12}{1 + F_3 + F_4} + 16F_2 - 4F_1^2 + 4F_2^2 - 8F_1 + 18\right\} - \frac{\sqrt{F_3 - F_4}}{1 + F_3 - F_4}\left\{\frac{32}{(1 + F_3 - F_4)^3} + \frac{32(F_2 - F_1) + 16}{(1 + F_3 - F_4)^2} + \frac{8\left[(F_2 - F_1)^2 + 2F_1\right] + 16(F_2 - F_1) + 12}{1 + F_3 - F_4}\right\}\right)\frac{\pi - 4\left(\tan^{-1}\sqrt{F_3 + F_4} - \tan^{-1}\sqrt{F_3 - F_4}\right)}{4}\Bigg] \tag{27}$$

The variation of $\left(C_{l_p}\right)_{CT}/A$ (eq. (27)) with the ratio $\frac{B/2}{H_1}$ for a fixed value of H/H_1 of 2 is shown in figure 4.

The side force resulting from the rolling motion may be determined utilizing the velocity potential and equation (21). In coefficient form this side force is given by

$$\left(C_{Y_p}\right)_{CT} = \frac{4A_v}{\pi\left(\sqrt{F_1} + \sqrt{-F_1 + 2F_2 + 4}\right)^3}\left[\int_0^{\sqrt{F_3 - F_4}} G(\zeta)d\zeta + \int_{\sqrt{F_3 + F_4}}^{\infty} G(\zeta)d\zeta\right] \tag{28}$$

where

$$G(\zeta) = \left\{\left[\frac{(F_1 - F_2 - 1)\zeta}{\zeta^2 + 1} - \frac{2\zeta}{(\zeta^2 + 1)^2}\right]\left[\pi - 4\left(\tan^{-1}\sqrt{F_3 + F_4} - \tan^{-1}\sqrt{F_3 - F_4}\right)\right] + \right.$$

$$\frac{4\zeta}{\zeta^2 + 1}\left(\frac{\sqrt{F_3 + F_4}}{1 + F_3 + F_4} - \frac{\sqrt{F_3 - F_4}}{1 + F_3 - F_4}\right) + \left[\frac{2F_2 - F_1 + F_1\zeta^2}{\zeta^2 + 1} + \right.$$

$$\left.\left.\frac{4}{(\zeta^2 + 1)^2}\right]\log_e \frac{\left(\sqrt{F_3 + F_4} + \zeta\right)\left(\sqrt{F_3 - F_4} - \zeta\right)}{\left(\sqrt{F_3 - F_4} + \zeta\right)\left(\sqrt{F_3 + F_4} - \zeta\right)}\right\} \frac{(F_1 - F_2)\zeta^3 + (F_1 - F_2 - 4)\zeta}{(\zeta^2 + 1)^2\sqrt{F_1\zeta^4 + 2F_2\zeta^2 - F_1 + 2F_2 + 4}}$$

The variation of $\left(C_{Y_p}\right)_{CT}/A_V$ with the ratio $\frac{B/2}{H_1}$ for a fixed value of H/H_1 of 2 has been determined by a numerical integration in the original plane and is presented in figure 5. With the lateral force known, the stability derivative C_{n_p} of the cruciform tail is easily obtained as pointed out in the section dealing with the pressures, forces, and moments.

Of special interest are the limiting expressions of equation (22) which represent the transformations to the ζ-plane of: (a) the crossflow plane of a pair of mutually bisecting, perpendicular surfaces and (b) the crossflow plane of an inverted T-tail.

Cruciform composed of two mutually bisecting, perpendicular, triangular surfaces.- In treating the cruciform with equal-span vertical panels, the cross section may be considered as having the same orientation in the complex plane as in the real plane; that is, H_1 is set equal to H and the horizontal tail has a span of $2H$ in both planes. In order that H_1 be equal to H, $\cos\theta_2$ must be set equal to $-\cos\theta_1$ in equations (23) with the result that

$$H = H_1 = 2\sqrt{1 - \cos^2\theta_1}$$

and

$$\frac{B}{2} = 2\cos\theta_1$$

If the same substitution is made in equation (22) and the local span of the horizontal panel is denoted as $b/2$, the transformation (eq. 22) may be written in the more useful form

$$Z = \frac{\pm\frac{b}{2}\sqrt{\zeta^4 - \frac{2(1 + \cos^2\theta_1)}{1 - \cos^2\theta_1}\zeta^2 + 1}}{\zeta^2 + 1} \tag{29}$$

The values of ζ at points ② and ④ (fig. 3(c)) are obtained from equation (29) as $\left(\frac{1 + \cos\theta_1}{1 - \cos\theta_1}\right)^{1/2}$ and $\left(\frac{1 - \cos\theta_1}{1 + \cos\theta_1}\right)^{1/2}$, respectively.

Let the parameter $\left(\frac{1 + \cos \theta_1}{1 - \cos \theta_1}\right)^{1/2}$ be defined as e. Equation (29) may then be simply expressed in the form

$$Z = \frac{\pm \frac{b}{2} \sqrt{\zeta^4 - \left(e^2 + \frac{1}{e^2}\right)\zeta^2 + 1}}{\zeta^2 + 1} \tag{30}$$

If the vertical panels are now given a span of $K\frac{b}{2}$, then

$$e = \sqrt{K^2 + 1} - K \tag{31}$$

and

$$e^2 + \frac{1}{e^2} = 4K^2 + 2 \tag{32}$$

The velocity potential for this case may be determined from equation (26) as

$$\phi = \frac{(b/2)^2 p}{\pi}\left[\frac{\zeta(\zeta^2 - 1)}{(\zeta^2 + 1)^2}\frac{(e^2 + 1)^2}{e^2}\left(2 \tan^{-1} e - \frac{\pi}{4}\right) + \right.$$

$$\left. \frac{\zeta^4 - \left(e^2 + \frac{1}{e^2}\right)\zeta^2 + 1}{(\zeta^2 + 1)^2} \log_e \frac{(1 + e\zeta)(e - \zeta)}{(1 - e\zeta)(e + \zeta)}\right] \tag{33}$$

Substituting for ζ in equation (33) the equivalent in terms of Z (determined from eq. (30)) yields the potential in the original plane for a cruciform of arbitrary dimensions. In the limiting cases where $K = 0$ or $K = 1$, this expression for the velocity potential reduces to that for the potentials given in references 2 and 3 for the rolling triangular wing and rolling equi-panel-span cruciform, respectively.

From equation (33) the pressure distributions and span loadings for K values of 0, 0.5, 0.75, and 1 have been determined and are presented in figures 6 and 7.

The damping-in-roll coefficient for this group of tails, which is obtained from equation (27) by making the proper substitutions for the cosine terms in terms of e, is found to be

$$\left(C_{l_p}\right)_{CT} = \frac{-A}{8}\left[-\left(\tan^{-1}e - \tan^{-1}\frac{1}{e} + \frac{\pi}{4}\right)\frac{(e^2 - 1)(e^4 - 6e^2 + 1)}{e^3} + \frac{\left(\tan^{-1}e - \tan^{-1}\frac{1}{e} + \frac{\pi}{4}\right)(1 + e^2)^4}{4e^4} + \frac{(e^2 - 1)^2}{e^2}\right] \tag{34}$$

The variation of $\left(C_{l_p}\right)_{CT}/A$ with K is plotted in figure 8.

Inverted T-tail.- By setting $\cos\theta_2 = -1$, the dimension H_1 of equation (23b) vanishes and the cruciform in the complex plane (fig. 3(b)) degenerates into the inverted T-tail. If the value of ζ at point ② for this case is designated as a, equation (22) reduces to

$$Z = \frac{4}{\sqrt{1 + a^2}}\frac{\zeta\sqrt{\zeta^2 - a^2}}{\zeta^2 + 1} \tag{35}$$

The proportions of the inverted T-tail will then be governed by the selection of a in the following equations:

$$\frac{B}{2} = \frac{2a^2}{1 + a^2} \tag{36a}$$

$$H = \frac{4}{\sqrt{1 + a^2}} \tag{36b}$$

$$R = \frac{H}{B} = \frac{\sqrt{1 + a^2}}{a^2} \tag{36c}$$

Equation (36c) may also be written as

$$a = \left(\frac{1 + \sqrt{1 + 4R^2}}{2R^2}\right)^{1/2} \tag{36d}$$

to allow for the selection of a for a desired value of R.

The velocity potential for an inverted T-tail of dimensions H and $B/2$ is found by a reduction of equation (26) and may be expressed as

$$\phi = \frac{16p}{(1 + a^2)\pi}\left\{\frac{\zeta^2(\zeta^2 - a^2)}{(\zeta^2 + 1)^2}\log_e\frac{\zeta + a}{\zeta - a} + \frac{\zeta\left[\zeta^2(3 + a^2) + 1 - a^2\right]}{(\zeta^2 + 1)^2}\left(\frac{\pi}{4} - \tan^{-1}a\right) + \frac{a\zeta}{\zeta^2 + 1}\right\} \tag{37}$$

A more general potential expression which will be valid for tails of dimensions h and $b/2$ may be evolved by multiplying the right-hand side of equation (37) by $(h/H)^2$ or $(b/B)^2$ and by altering the transformation formula so that on the vertical panel

$$\zeta = \pm\left\{\frac{2\left(\frac{z}{h}\right)^2 + a^2 + \sqrt{a^4 + 4\left(\frac{z}{h}\right)^2(a^2 + 1)}}{2\left[1 - \left(\frac{z}{h}\right)^2\right]}\right\}^{1/2} \tag{38a}$$

and on the horizontal tail

$$\zeta = \pm\left[\frac{\frac{-a^2}{a^2 + 1}\left(\frac{y}{b/2}\right)^2 + 2 \pm 2\sqrt{1 - \left(\frac{y}{b/2}\right)^2}}{\frac{4}{a^2} + \frac{a^2}{a^2 + 1}\left(\frac{y}{b/2}\right)^2}\right]^{1/2} \tag{38b}$$

The spanwise pressure distribution may be determined from equation (12) together with the potential for the rolling inverted T-tail of dimensions h and b/2. The pressure distributions for various values of R are plotted in figure 9; spanwise loadings are presented for these same values of R in figure 10.

The following expression for $\left(C_{Y_p}\right)_{TT}$ is obtained from equation (28) when $\cos \theta_2 = -1$:

$$\left(C_{Y_p}\right)_{TT} = -A_V\left[\frac{a(5a^2 + 3)}{3(a^2 + 1)^{3/2}} + \frac{(a^2 + 1)^{1/2}(\pi - 4 \tan^{-1}a)}{4}\right] \tag{39}$$

Figure 11 represents the variation of $\left(C_{Y_p}\right)_{TT}/A_V$ with the parameter R

The damping-in-roll coefficient nondimensionalized with respect to the horizontal-tail area is given by

$$\left(C_{l_p}\right)_{TT} = \frac{-A(1 + a^2)^2}{2\pi a^8}\left[\frac{(a^4 + 2a^2 + 9)(\pi - 4 \tan^{-1}a)^2}{16} + \frac{a(a^2 - 9)(4 \tan^{-1}a - \pi)}{2} + \frac{(a^4 + 14a^2 + 9)a^2}{(a^2 + 1)^2}\right] \tag{40}$$

The variation of $\left(C_{l_p}\right)_{TT}/A$ with R has been shown in figure 12 to depict the effect the addition of a vertical panel to a slender triangular tail has on the rolling characteristics of the tail.

Rolling V-tails.- The expression necessary to transform a V-tail and the region exterior to it to the infinite straight-line plane can be obtained from reference 11 and is

$$Z = \frac{4(-\zeta^2)^{\frac{1-\sigma}{2}}}{\zeta^2 + 1} \tag{41}$$

where σ defines the "dihedral" angle τ (see fig. 13) as

$$\tau = \frac{\pi\sigma}{2} \tag{42}$$

and the span of the tail panels as

$$\frac{B}{2} = 2(1 - \sigma^2)^{1/2}\left(\frac{1 + \sigma}{1 - \sigma}\right)^{\sigma/2} \tag{43}$$

The positioning of the V-tail in the complex plane, as well as the correspondence of points in the Z- and ζ-planes, may be seen in figure 13.

In order to note the effect on the forces and moments of changing the dihedral angle, tails with dihedral angles of 22.5°, 45°, and 67.5°, in addition to the two limiting cases of 0° and 90°, have been investigated. The auxiliary function $h(\xi)$ and the velocity potential in the ζ-plane are listed in the following table for each of the five tails:

τ, deg	$h(\xi)$	$\phi \Big/ p\left(\frac{b}{2}\right)^2$
0	$16\xi^2$	$\frac{\zeta(1 - \zeta^2)}{(\zeta^2 + 1)^2}$
22.5	$16\xi^{3/2}$	$\frac{\sqrt{2}}{(2.064)^2}\,\frac{\zeta(-\zeta^2 - 3\zeta + 3) + 1}{(\zeta^2 + 1)^2}$
45	16ξ	$\frac{4}{3\sqrt{3}}\,\frac{1 - \zeta^2}{(\zeta^2 + 1)^2}$
67.5	$16\xi^{1/2}$	$\frac{\sqrt{2}}{(2.744)^2}\,\frac{-\zeta(\zeta^2 + \zeta + 5) + 3}{(\zeta^2 + 1)^2}$
90	16	$\frac{-\zeta(\zeta^2 + 3)}{4(\zeta^2 + 1)^2}$

In order to show the various end-plate effects, trailing-edge potentials, as well as span loadings, have been plotted in figure 14. For comparative purposes the span loading for the equi-panel-span cruciform has also been included. The variation of $\left(C_{l_p}\right)_{VT}/A'$ and $\left(C_{Y_p}\right)_{VT}/A'$ with τ is plotted in figure 15. This figure shows that, theoretically, V-tails with dihedral angles in the immediate vicinity of 45° yield more damping than a cruciform tail which has twice the damping-surface area.

Rolling Y-tail.- The velocity potential for a rolling Y-tail with any desired ratio of the span of the arms to the span of the stem (vertical panel) may be readily determined by the method presented in this report. The Y-tail considered in the following analysis has an angle of 90° between the two arms and an angle of 135° between the arms and the stem (fig. 16(a)).

The expression required to transform the Y-tail and the region exterior to it to the infinite straight-line plane can be obtained from reference 10 as

$$Z = \frac{\left[8(1 - \cos \theta_1)^3\right]^{1/4}(\zeta^2 - e^2)^{3/4}(2\zeta)^{1/2}}{\zeta^2 + 1} \tag{44}$$

where e, as before, is defined as $\left(\frac{1 + \cos \theta_1}{1 - \cos \theta_1}\right)^{1/2}$. The orientation of the Y-tail in the Z-plane and the correspondence of the points in the Z- and ζ-planes are shown in figure 16. The dimensions of the Y-tail are obtained by the selection of $\cos \theta_1$ in the following equations:

$$\frac{B}{2} = \frac{(27)^{1/4}}{2}(1 + \cos \theta_1) \tag{45a}$$

$$H = 2\left[2(1 - \cos \theta_1)^3\right]^{1/4} \tag{45b}$$

The required $h(\xi)$ functions are

$$4\sqrt{2(1 - \cos\theta_1)^3}\,\xi(e^2 - \xi^2)^{3/2}$$

and

$$4\sqrt{2(1 - \cos\theta_1)^3}\,\xi(\xi^2 - e^2)^{3/2}$$

on the arms and stem, respectively. Substituting these functions into equation (20b) and integrating over the proper portions of the boundary (see fig. 16) yield the complex potential in the ζ-plane as

$$W = 2\sqrt{2(1 - \cos\theta_1)^3}\,p\left[\frac{\zeta\sqrt{1 + e^2}(3\zeta^2 + 1 - 2e^2)}{2(\zeta^2 + 1)^2} + \right.$$

$$1 + \frac{\sqrt{1 + e^2}}{2}\,\frac{-\zeta^2(4 + e^2) + e^2 - 2}{(\zeta^2 + 1)^2} + \frac{i\zeta(e^2 - \zeta^2)^{3/2}}{(\zeta^2 + 1)^2} +$$

$$\left.\frac{i\zeta(\zeta^2 - e^2)^{3/2}}{(\zeta^2 + 1)^2}\right] \tag{46}$$

The nondimensional velocity-potential parameter on the arms is

$$\frac{\phi}{p(b/2)^2} = \frac{8\sqrt{2(1 - \cos\theta_1)^3}\,\sqrt{1 + e^2}}{3\sqrt{3}(1 + \cos\theta_1)^2}\left[\frac{\zeta(3\zeta^2 + 1 - 2e^2)}{2(\zeta^2 + 1)^2} + \frac{1}{\sqrt{1 + e^2}} + \right.$$

$$\left.\frac{-\zeta^2(4 + e^2) + e^2 - 2}{2(\zeta^2 + 1)^2} + \frac{\zeta(e^2 - \zeta^2)^{3/2}}{\sqrt{1 + e^2}(\zeta^2 + 1)^2}\right] \tag{47}$$

and on the stem or vertical panel is

$$\frac{\phi}{ph^2} = \frac{\sqrt{1+e^2}}{2}\left[\frac{\zeta(3\zeta^2+1-2e^2)}{2(\zeta^2+1)^2} + \frac{1}{\sqrt{1+e^2}} + \frac{-\zeta^2(4+e^2)+e^2-2}{2(\zeta^2+1)^2} - \frac{\zeta(\zeta^2-e^2)^{3/2}}{\sqrt{1+e^2}(\zeta^2+1)^2}\right] \tag{48}$$

In the limiting cases $\cos\theta_1 = 1$ and -1 the potentials are obtained for the rolling V-tail with a dihedral angle of 45° and for a triangular panel rolling about one edge, respectively. Sample trailing-edge potentials and span loadings are presented in figures 17 and 18.

For convenience, only numerical integrations were made of the span loadings to obtain the side force and rolling moment due to rolling. These results have been nondimensionalized and are presented as the parameters $\left(C_{Y_p}\right)_{YT}/A'$ and $\left(C_{l_p}\right)_{YT}/A'$ in figure 19.

Figure 20 has been prepared to illustrate the relative damping qualities of the various tail arrangements of panels of the same span and area considered in this paper. The relative merit of the Y-tail as shown in this figure may be of particular interest.

Cruciform tail-body arrangement.- The method presented herein can easily be applied to a cruciform tail-body arrangement to determine the integral solution of the complex potential in the ζ-plane. No effort was made to evaluate the integrals; therefore, the analytical expression for the potential and, hence, the associated pressures and span loadings are not presented for this case. Nevertheless, the development of the integral form of the complex potential in the ζ-plane was considered of sufficient interest to warrant presentation herein.

The contour of the cruciform tail-body configuration shown in figure 21(a) may be transformed to a pair of mutually bisecting, perpendicular, triangular surfaces by an application of the Joukowski transformation (fig. 21(b)) and then to the infinite straight line (fig. 21(c)) by use of a transformation similar to the one used in

the previous illustrations. This procedure results in the following relation between Z and ζ:

$$Z = \frac{\frac{(b/2)^2 + r_o^2}{2b/2}\left(\zeta^4 - 2\left\{\frac{2\left[K^2(b/2)^2 - r_o^2\right]^2}{K^2\left[(b/2)^2 + r_o^2\right]^2} + 1\right\}\zeta^2 + 1\right)^{1/2}}{\zeta^2 + 1} \pm$$

$$\frac{\left[\frac{\left[(b/2)^2 + r_o^2\right]^2}{4(b/2)^2}\left(\zeta^4 - 2\left\{\frac{2\left[K^2(b/2)^2 - r_o^2\right]^2}{K^2\left[(b/2)^2 + r_o^2\right]^2} + 1\right\}\zeta^2 + 1\right) - 4r_o^2(b/2)^2(\zeta^2 + 1)^2\right]^{1/2}}{\zeta^2 + 1} \quad (49)$$

On the vertical and horizontal panels both terms will be real or both imaginary; whereas, on the body the first term will be real and the second imaginary.

As noted previously, in order to determine the complex potential, the $h(\xi)$ function must be substituted into equation (11) and integrated over the boundary. The $h(\xi)$ functions over the portions of the boundary corresponding to the horizontal and vertical panels (see fig. 21) will be plus and minus $\left[f_1(\xi) + f_2(\xi)\right]^2$, respectively, where $f_1(\xi)$ is the numerator of the first term of equation (49) and $f_2(\xi)$ is the numerator of the second term. The $h(\xi)$ function over the portions of the boundary corresponding to the body is $\left[f_1(\xi)\right]^2 - \left[f_2(\xi)\right]^2$. The integral equation for the complex potential is then

$$W = \frac{p}{2\pi}\left(\int_{①}^{⑫} \frac{\left[f_1(\xi) + f_2(\xi)\right]^2 d\xi}{(\xi^2+1)^2(\xi-\zeta)} + \int_{⑫}^{⑪} \frac{\left\{\left[f_1(\xi)\right]^2 - \left[f_2(\xi)\right]^2\right\} d\xi}{(\xi^2+1)^2(\xi-\zeta)} - \right.$$

$$\int_{⑪}^{⑨} \frac{\left[f_1(\xi) + f_2(\xi)\right]^2 d\xi}{(\xi^2+1)^2(\xi-\zeta)} + \int_{⑨}^{⑧} \frac{\left\{\left[f_1(\xi)\right]^2 - \left[f_2(\xi)\right]^2\right\} d\xi}{(\xi^2+1)^2(\xi-\zeta)} +$$

$$\int_{⑧}^{⑥} \frac{\left[f_1(\xi) + f_2(\xi)\right]^2 d\xi}{(\xi^2+1)^2(\xi-\zeta)} + \int_{⑥}^{⑤} \frac{\left\{\left[f_1(\xi)\right]^2 - \left[f_2(\xi)\right]^2\right\} d\xi}{(\xi^2+1)^2(\xi-\zeta)} -$$

$$\int_{⑤}^{③} \frac{\left[f_1(\xi) + f_2(\xi)\right]^2 d\xi}{(\xi^2+1)^2(\xi-\zeta)} + \int_{③}^{②} \frac{\left\{\left[f_1(\xi)\right]^2 - \left[f_2(\xi)\right]^2\right\} d\xi}{(\xi^2+1)^2(\xi-\zeta)} +$$

$$\left.\int_{②}^{①} \frac{\left[f_1(\xi) + f_2(\xi)\right]^2 d\xi}{(\xi^2+1)^2(\xi-\zeta)}\right) \tag{50}$$

where the values of ξ as determined from equation (49) at the points ⑫, ⑧, ⑥, and ② (fig. 21(c)) are given by

$$\xi = \pm \left\{ \frac{4r_o^2 + \left\{ \frac{2\left[K^2(b/2)^2 - r_o^2\right]^2}{K^2\left[(b/2)^2 + r_o^2\right]^2} + 1 \right\} \left(\frac{b}{2} + \frac{r_o^2}{b/2} \right)^2}{\left(\frac{b}{2} + \frac{r_o^2}{b/2} \right)^2 - 4r_o^2} \pm \right.$$

$$\left. \frac{\left[\left(\frac{b}{2} + \frac{r_o^2}{b/2} \right)^4 \left(\left\{ \frac{2\left[K^2(b/2)^2 - r_o^2\right]^2}{K^2\left[(b/2)^2 + r_o^2\right]^2} + 1 \right\}^2 - 1 \right) + 16r_o^2 \left(\frac{b}{2} + \frac{r_o^2}{b/2} \right)^2 \left\{ \frac{\left[K^2(b/2)^2 - r_o^2\right]^2}{K^2\left[(b/2)^2 + r_o^2\right]^2} + 1 \right\} \right]^{1/2}}{\left(\frac{b}{2} + \frac{r_o^2}{b/2} \right)^2 - 4r_o^2} \right\}^{1/2} \tag{51}$$

at the points ③ and ⑪ by

$$\xi = \pm \left(\left\{ \frac{\left[K^2(b/2)^2 - r_o^2\right]^2}{K^2\left[(b/2)^2 + r_o^2\right]^2} + 1 \right\}^{1/2} - \frac{K^2(b/2)^2 - r_o^2}{K\left[(b/2)^2 + r_o^2\right]} \right) \tag{52}$$

and at the points ⑨ and ⑤ by the reciprocal of equation (52).

Approximation of the Rolling Stability Derivatives

For many arrangements, because of the inherent difficulties involved in making a rigorous estimate of the stability derivative C_{Y_p} $\left(\text{and hence, } C_{l_p} \text{ and } C_{n_p}\right)$, an approximation to this derivative based on a knowledge of the aerodynamic loading due to sideslip becomes necessary. In the simplest of these approximations, β is assumed to be equal to the average angle of attack due to rolling $ph/2V$. In a second and more accurate approximation β is assumed to be equal to the spanwise distance to the center of pressure of the sideslipping tail multiplied by p/V. If C_{Y_p} is expressed in the form

$$C_{Y_p} = \frac{\partial C_Y}{\partial \beta} \frac{\partial \beta}{\partial\left(\frac{ph}{V}\right)} \tag{53}$$

the first approximation is

$$C_{Y_p} = \frac{1}{2} C_{Y_\beta} \tag{54}$$

and the second approximation is

$$C_{Y_p} = \frac{\bar{z}}{h} C_{Y_\beta} \tag{55}$$

where $\bar{z}$ is the spanwise distance to the center of pressure.

An indication of the accuracy of these approximations may be obtained by a consideration of the inverted T-tail. A theoretical estimate of C_{Y_β} for an inverted T-tail may be determined from reference 12 and can be expressed as

$$\left(C_{Y_\beta}\right)_{TT} = \frac{\pi}{2} A_V \frac{1 + 2a^2}{1 + a^2} \tag{56}$$

This expression together with equation (39) provides an interesting theoretical check on the accuracy of the preceding approximations when applied to a slender inverted T-tail.

The correction factor given by the ratio of equation (39) to equation (56) is

$$\frac{\left(C_{Y_p}\right)_{TT}}{\left(C_{Y_\beta}\right)_{TT}} = \frac{4a(5a^2 + 3) + 3(a^2 + 1)^2(\pi - 4 \tan^{-1}a)}{6\pi(a^2 + 1)^{1/2}(1 + 2a^2)} \tag{57}$$

This ratio is compared in figure 22 with the approximations given by equations (54) and (55). The values of $\left(C_{Y_p}\right)_{TT}$ obtained from equations (54) and (55) are presented in figure 11. It may be noted that equation (55) gives excellent agreement (within 5 percent) with the exact values of $\left(C_{Y_p}\right)_{TT}$ for values of R greater than 2. For values of R less than 2 an estimation of $\left(C_{Y_p}\right)_{TT}$ based on the approximation obtained by equation (55) may not be advisable.

As a point of interest, the variation of $\left(C_{Y_\beta}\right)_{TT}/A_V$ and $\left(C_{l_\beta}\right)_{TT}/A$ (determined from ref. 12) with R is presented in figures 23 and 24. The expression for $\left(C_{l_\beta}\right)_{TT}$ is

$$\left(C_{l_\beta}\right)_{TT} = \frac{A}{4}\left\{\frac{32}{3a^2} + \frac{2(1 + a^2)^2}{a^6}\left[\frac{2a(1 - a^2)}{(1 + a^2)^2} - \cos^{-1}\frac{1 - a^2}{1 + a^2}\right] + \frac{\pi(1 + a^2)^2}{a^6}\right\} \tag{58}$$

Effect of the Wing Flow Field on the Tail Characteristics

In order to make an accurate estimate of the derivatives C_{l_p} and C_{n_p} for a complete wing-tail-body configuration similar to present-day missiles, the effect of the wing flow field on the tail must be considered. The importance of these effects for a rolling wing-tail combination is simply illustrated by an approximate determination of the downwash and sidewash velocities induced on a slender inverted T-tail by a slender, rolling, triangular wing (see fig. 25).

The perturbated downwash and sidewash velocities were obtained in a plane perpendicular to the free stream at an infinite distance downstream of the wing. Although the wing is of low aspect ratio, the

trailing vortex sheet has been assumed to remain flat. Even though the vortex sheet may actually roll up, no theoretical or experimental evidence is available to indicate the aspect ratios or rotational speeds at which this rolling up will occur. A further assumption is that, for the usual values of $pb/2V$ encountered and for tail lengths of practical magnitude, the rotation of the vortex sheet at the tail location can be neglected.

Based upon the preceding assumptions, the downwash and sidewash determined from the Biot-Savart equation are formulated as follows:

$$w(\infty,y_1,0) = \frac{1}{2\pi}\frac{1}{b/2}\int_{-1}^{1}\frac{d\Gamma}{dy_2}\frac{dy_2}{y_2 - y_1} \tag{59}$$

$$v(\infty,0,z_1) = \frac{z_1}{2\pi}\frac{1}{b/2}\int_{-1}^{1}\frac{d\Gamma}{dy_2}\frac{dy_2}{z_1^2 + y_2^2} \tag{60}$$

For a slender triangular wing (ref. 5), the rate of change of the circulation with respect to y_2 is

$$\frac{d\Gamma}{dy_2} = V\frac{b}{2}\frac{pb}{2V}\frac{1 - 2y_2^2}{\sqrt{1 - y_2^2}} \tag{61}$$

Substituting equation (61) into equations (59) and (60), performing the integration, and taking the partial derivative with respect to $pb/2V$ give

$$\frac{\partial\frac{w}{V}}{\partial\frac{pb}{2V}} = -y_1 \qquad (|y_1| < 1) \tag{62}$$

and

$$\frac{\partial \frac{v}{V}}{\partial \frac{pb}{2V}} = \frac{1}{2}\left(\frac{1 + 2z_1^2}{\sqrt{1 + z_1^2}} - 2z_1\right) \qquad (z_1 > 0) \qquad (63)$$

The induced downwash (eq. (62)) will equal both in magnitude and direction the downwash due to rolling of the horizontal tail which is

$$w = -py = -\frac{pb}{2V} V \frac{y}{b/2} \qquad (64)$$

From equation (64) it follows that

$$\frac{\partial \frac{w}{V}}{\partial \frac{pb}{2V}} = -y_1 \qquad (65)$$

The damping force resulting from the difference of these two perturbated velocities (eq. (65) minus eq. (62)) will therefore be zero. The induced sidewash from the wing exerts a side force on the vertical panel of the tail in opposition to the side force produced by the isolated tail; hence, the effect of the wing sidewash is to decrease the amount of tail damping. This decrease will be rather large for most wing-tail arrangements and it is possible for the induced force to be greater than the damping force of the isolated tail with the result that the vertical tail contributes an antidamping force to the system. For the illustrative example the induced side force on the vertical panel is approximately 82 percent as large as the side force due to rolling. The damping in roll of the tail immersed in the flow field behind the wing is of the order of 15 percent of the value predicted for the tail alone. The induced angle of attack on the vertical panel, the angle of attack due to rolling, and the resultant effective angle of attack are plotted in figure 25.

CONCLUDING REMARKS

A method, based on conformal-transformation techniques, for solving two-dimensional boundary-value problems has been used to evaluate the

velocity potentials, span loadings, pressure distributions, and associated stability derivatives for several slender-tail arrangements. Illustrative variations of the rolling stability derivatives for several series of tail shapes, as well as sample span loadings and pressure distributions, are included.

Two simple approximations of the rolling stability derivatives have been examined in view of the exact values determined by the method presented in this report. In addition, the importance of wing-tail interference has been shown with the aid of some elementary flow-field calculations.

Langley Aeronautical Laboratory,
National Advisory Committee for Aeronautics,
Langley Field, Va., March 17, 1953.

APPENDIX

DERIVATION OF THE EQUATION FOR THE COMPLEX POTENTIAL

The purpose of this analysis is to derive the equation (eq. (10) in the body of the paper)

$$W(\zeta) = \phi + i\psi = -\frac{1}{\pi}\int_{-\infty}^{\infty}\frac{\psi(\xi)d\xi}{\xi - \zeta}$$

from a knowledge of the general solution of the Riemann-Hilbert problem for the half plane. The Riemann-Hilbert problem is formulated as follows: A function $W(\zeta) = \phi(\zeta) + i\psi(\zeta)$ must be found which is regular in the upper half plane $(\eta > 0)$, bounded at infinity, and satisfies, on the infinite real axis L, the boundary condition

$$l(\xi)\phi(\xi) - m(\xi)\psi(\xi) = n(\xi) \tag{A1}$$

where $l(\xi)$, $m(\xi)$, and $n(\xi)$ are real continuous functions of ξ given on L. The functions are assumed to satisfy the Hölder condition on L (see refs. 10 and 13) and the additional condition that $l^2 + m^2 \neq 0$ for all values of ξ including $\xi = \infty$. In regard to the Hölder condition, a function, say $m(\xi)$, will satisfy this condition on L if, for any two points, ξ_1, ξ_2 on L,

$$\left|m(\xi_2) - m(\xi_1)\right| \leqq A\left|\xi_2 - \xi_1\right|^{\mu}$$

where A and μ are positive constants. The constant A is called the Hölder constant and μ the Hölder index. This definition of the Hölder condition has been obtained from reference 10.

The general solution of the Riemann-Hilbert problem under the conditions stipulated has been presented by N. I. Muskhelishvili in the following form (see ref. 10):

$$W(\zeta) = \frac{X(\zeta)}{\pi i}\int_{-\infty}^{\infty}\frac{n(\xi)d\xi}{X^{+}(\xi)\left[l(\xi) + im(\xi)\right](\xi - \zeta)} + (\text{Constant})X(\zeta) \tag{A2}$$

where $X(\zeta)$ is the fundamental solution of the associate homogeneous problem and

$$X^+(\xi) = \lim_{\eta \to 0^+} X(\zeta)$$

The fundamental solution $X(\zeta)$ in terms of the boundary conditions is given by

$$X(\zeta) = e^{\Gamma(\zeta)}$$

where

$$\Gamma(\zeta) = \frac{1}{2\pi} \int_{-\infty}^{\infty} \frac{\tan^{-1}\left(-\frac{l - im}{l + im}\right) d\xi}{\xi - \xi_0}$$

and

$$\xi_0 = \lim_{\eta \to 0^+} \zeta$$

Now, for the boundary conditions considered in this paper, it is necessary to set $l(\xi) = 0$ and $m(\xi) = -1$; hence, $n(\xi) = \psi(\xi)$. It follows that

$$X(\zeta) = -i$$

$$X^+(\zeta) = -i$$

and the general solution expressed by equation (A2) resolves into

$$W(\zeta) = \frac{1}{\pi} \int_{-\infty}^{\infty} \frac{\psi(\xi) d\xi}{\xi - \zeta} + i(\text{Constant}) \qquad (A3)$$

which is the Bickley relation (except for constant term) that is presented as equation (10) in the body of the paper. The constant term of equation (A3), however, is zero for the boundary conditions considered herein, since the imaginary part of $W(\zeta)$ as $\zeta \to \xi$ must equal $\psi(\xi)$.

REFERENCES

1. Jones, Robert T.: Properties of Low-Aspect-Ratio Pointed Wings at Speeds Below and Above the Speed of Sound. NACA Rep. 835, 1946. (Supersedes NACA TN 1032.)

2. Ribner, Herbert S.: The Stability Derivatives of Low-Aspect-Ratio Triangular Wings at Subsonic and Supersonic Speeds. NACA TN 1423, 1947.

3. Adams, Gaynor J.: Theoretical Damping in Roll and Rolling Effectiveness of Slender Cruciform Wings. NACA TN 2270, 1951.

4. Spreiter, John R.: The Aerodynamic Forces on Slender Plane- and Cruciform-Wing and Body Combinations. NACA Rep. 962, 1950. (Supersedes NACA TN's 1897 and 1662.)

5. Lomax, Harvard, and Heaslet, Max. A.: Damping-in-Roll Calculations for Slender Swept-Back Wings and Slender Wing-Body Combinations. NACA TN 1950, 1949.

6. Ribner, Herbert S.: Damping in Roll of Cruciform and Some Related Delta Wings at Supersonic Speeds. NACA TN 2285, 1951.

7. Westwater, F. L.: Some Applications of Conformal Transformations to Airscrew Theory. Proc. Cambridge Phil. Soc., vol. 32, pt. 4, Oct. 1936, pp. 676-684.

8. Bickley, W. G.: Two-Dimensional Potential Problems Concerning a Single Closed Boundary. Phil. Trans. Roy. Soc. (London), ser. A, vol. 228, 1929, pp. 235-274.

9. Lomax, Harvard, and Heaslet, Max. A.: Linearized Lifting-Surface Theory for Swept-Back Wings With Slender Plan Forms. NACA TN 1992, 1949.

10. Muskhelishvili, N. I.: Singular Integral Equations. Boundary Problems of Function Theory and Their Application to Mathematical Physics (Second ed., 1946). Translation No. 12, Aero. Res. Labs., Dept. Supply and Dev., Commonwealth of Australia, Feb. 1949.

11. Rotta, J.: Luftkräfte am Tragflügel mit einer seitlichen Scheibe. Ing.-Archiv, Bd. XIII, Heft 3, June 1942, pp. 119-131.

12. Katzoff, S., and Mutterperl, William: The End-Plate Effect of a Horizontal-Tail Surface on a Vertical-Tail Surface. NACA TN 797, 1941.

13. Kellogg, Oliver Dimon: Foundations of Potential Theory. Fredrick Ungar Publishing Co. (New York), 1929.

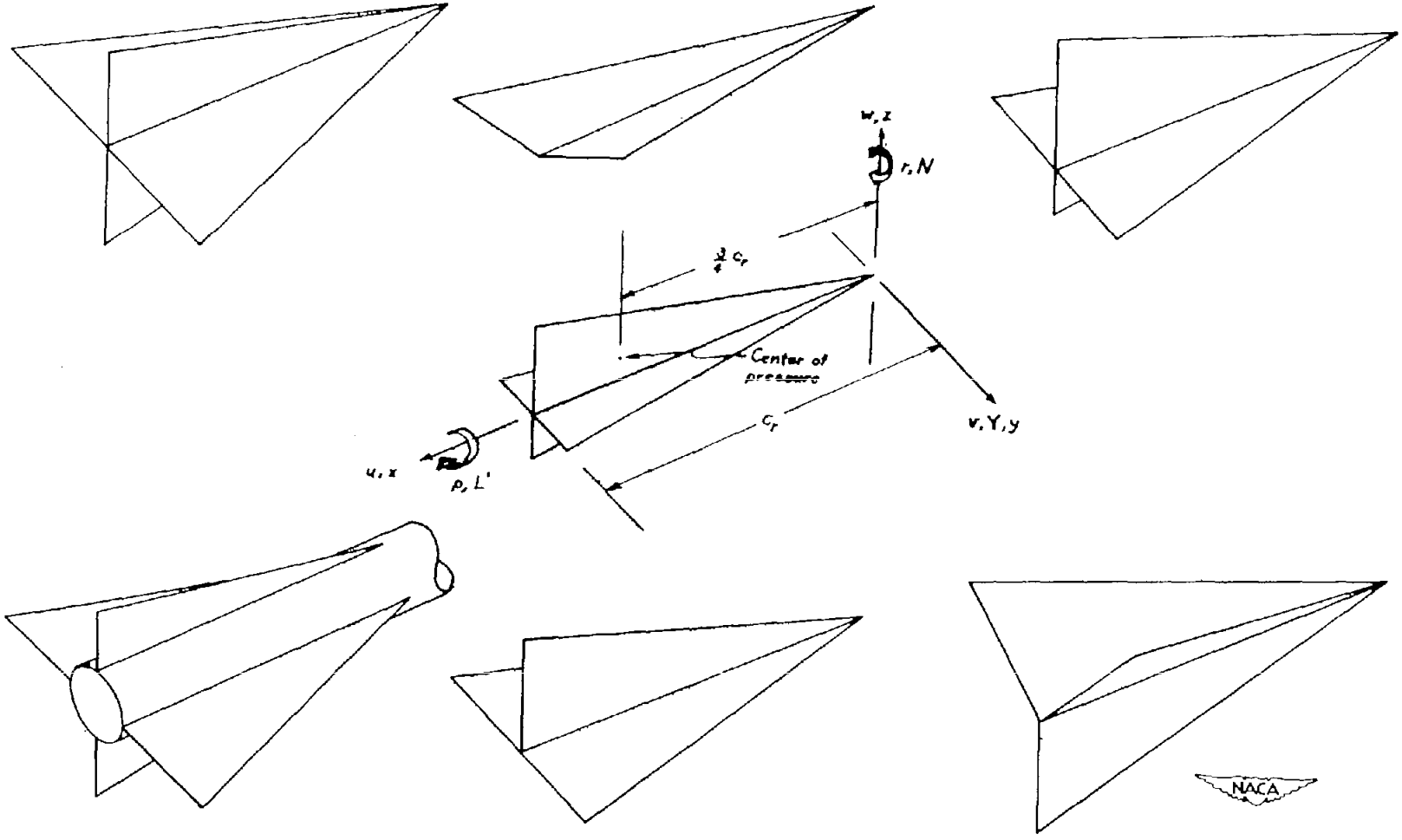

Figure 1.- Typical tail arrangements considered in the analysis. Center tail arrangement illustrates the system of axes used and the positive direction of the velocities, moments, and lateral force.

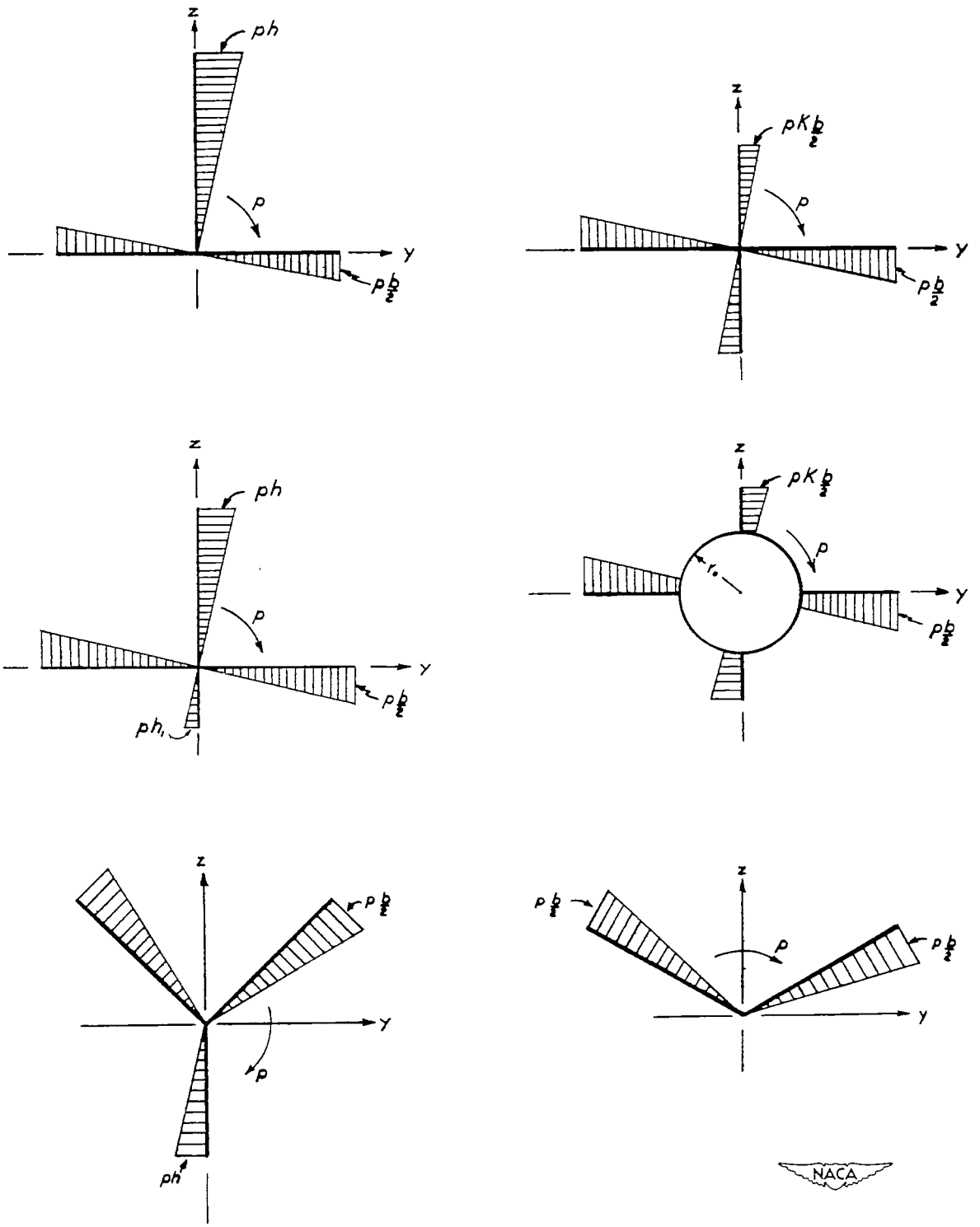

Figure 2.- Boundary conditions on tail arrangements for steady rolling motion.

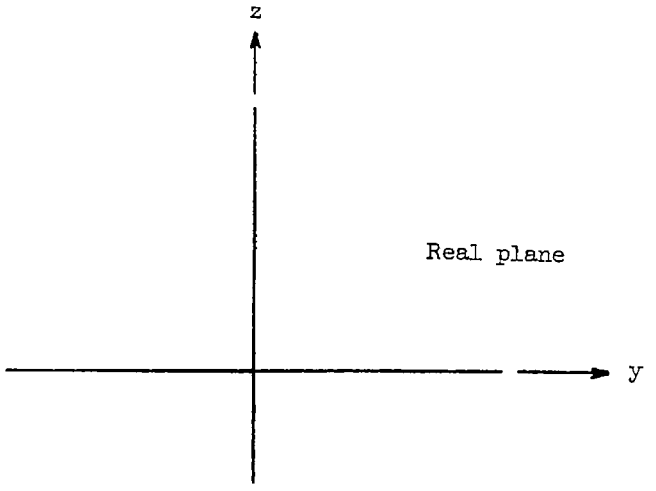

(a) Cross section of cruciform in physical plane.

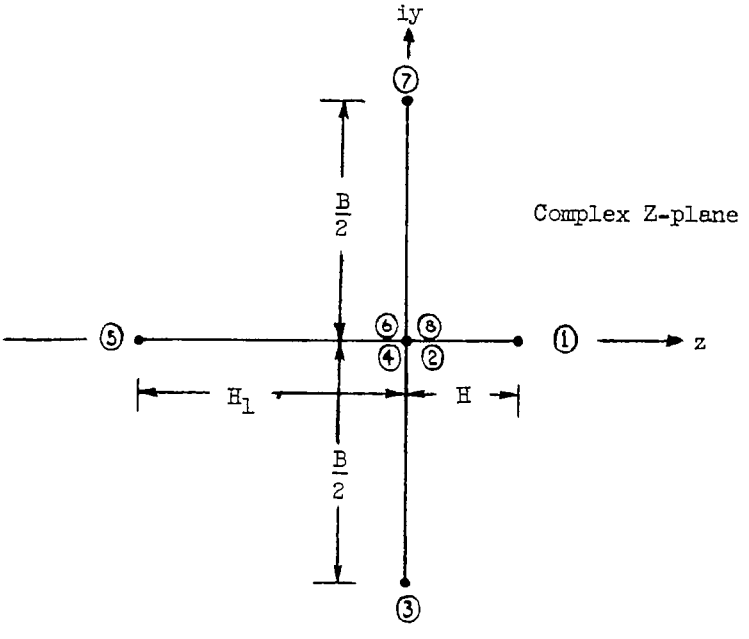

(b) Cruciform oriented for two-dimensional analysis.

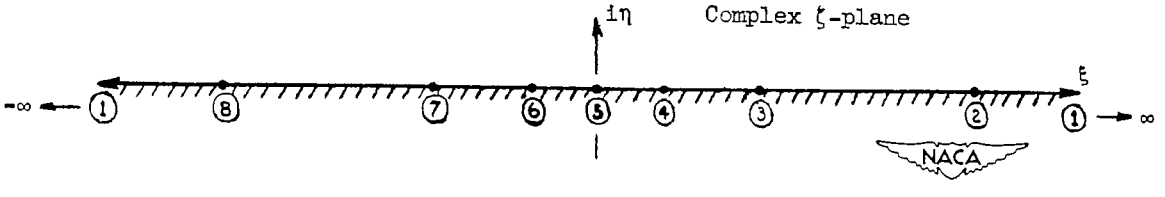

(c) Points in the ζ-plane corresponding to the vertices in the Z-plane.

Figure 3.- Physical and transformed planes used in analysis of rolling tails.

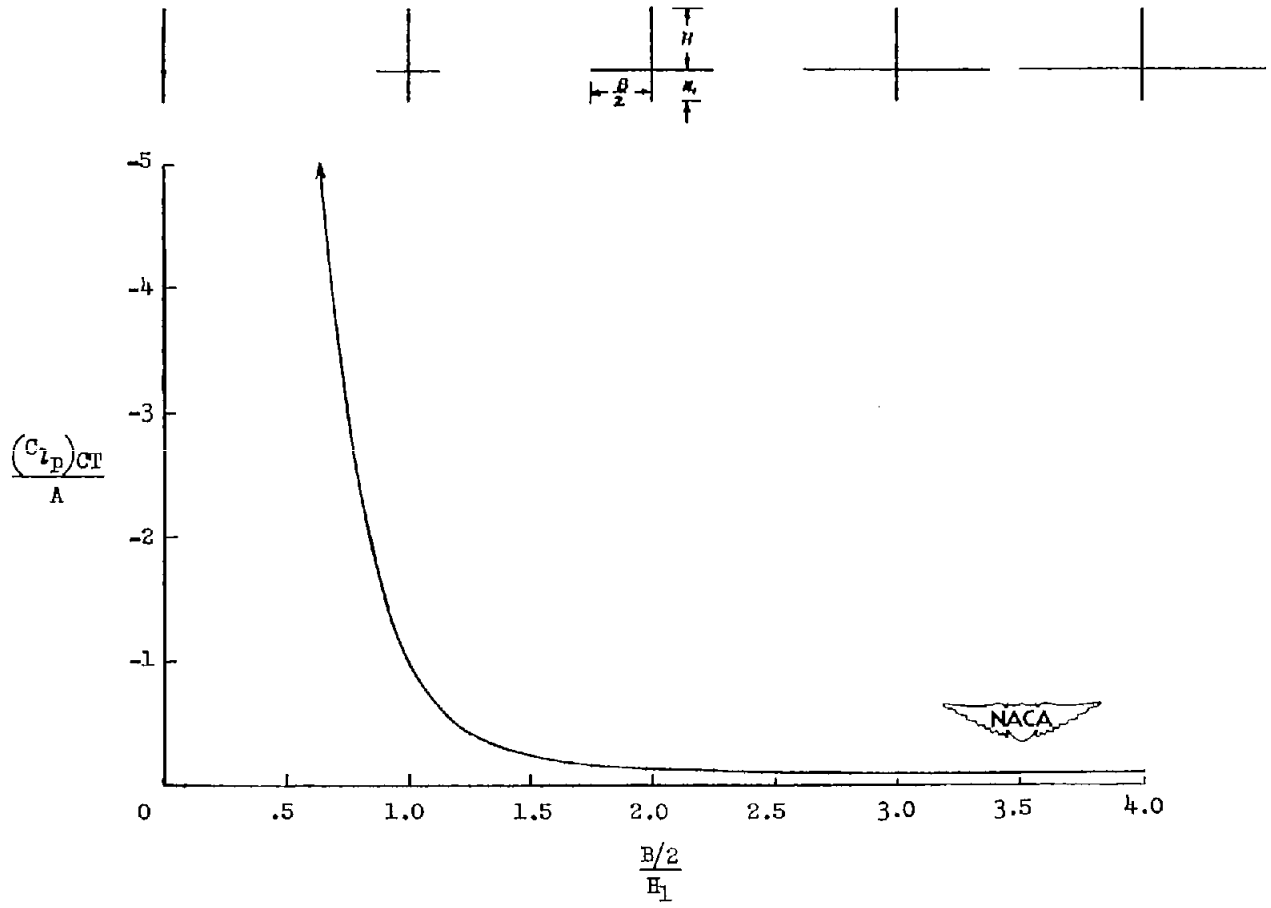

Figure 4.- The damping in roll of a slender cruciform tail for various values of $\frac{B/2}{H_1}$ and a fixed value of 2 for the ratio H/H_1. As $\frac{B/2}{H_1} \longrightarrow \infty$, C_{l_p}/A approaches the slender-tail value of $-\pi/32$.

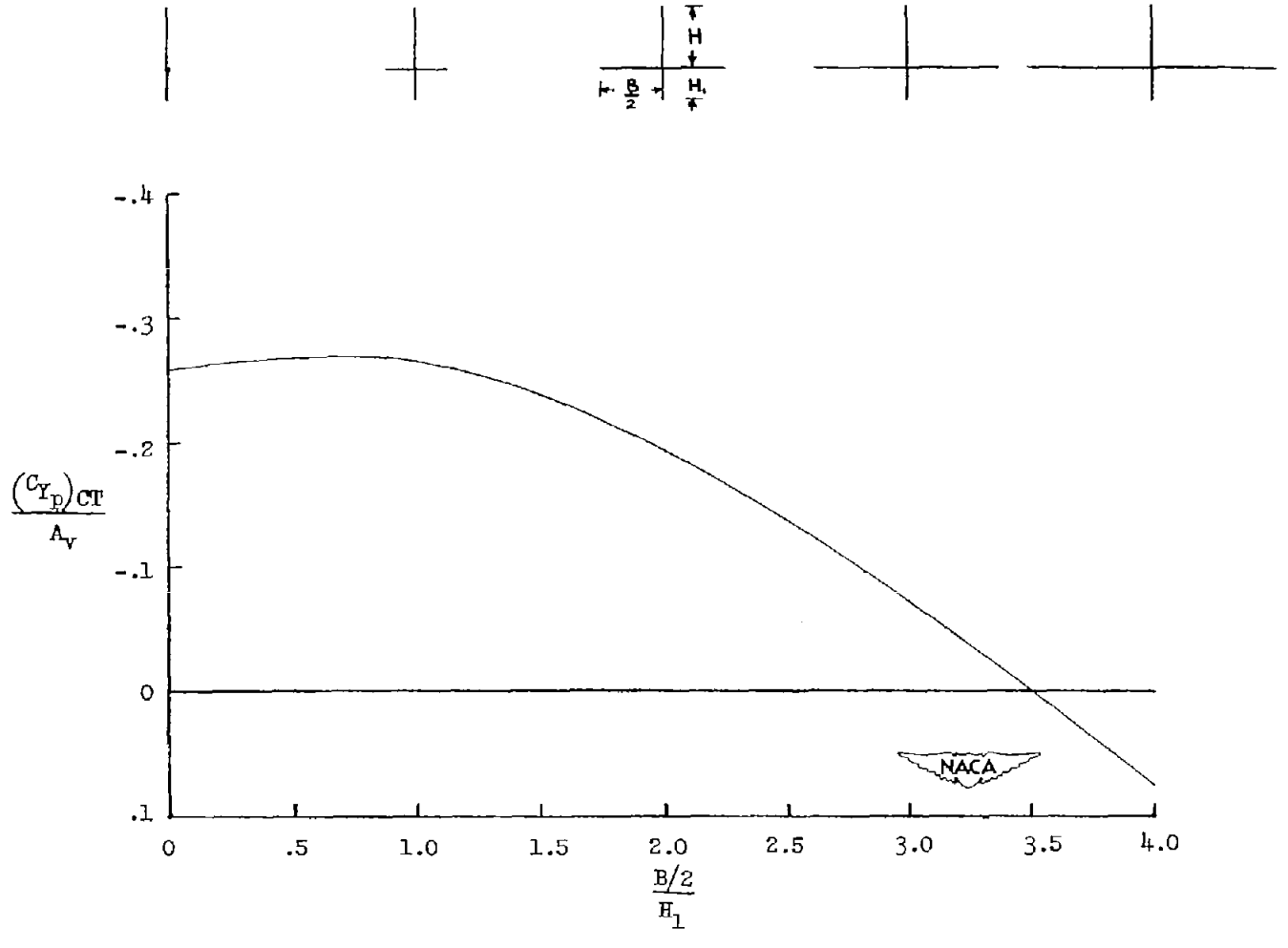

Figure 5.- The effect on the side force due to rolling of a slender cruciform tail of increasing the horizontal-tail span while maintaining the ratio of the upper-vertical-panel span to the lower-vertical-panel span equal to 2.

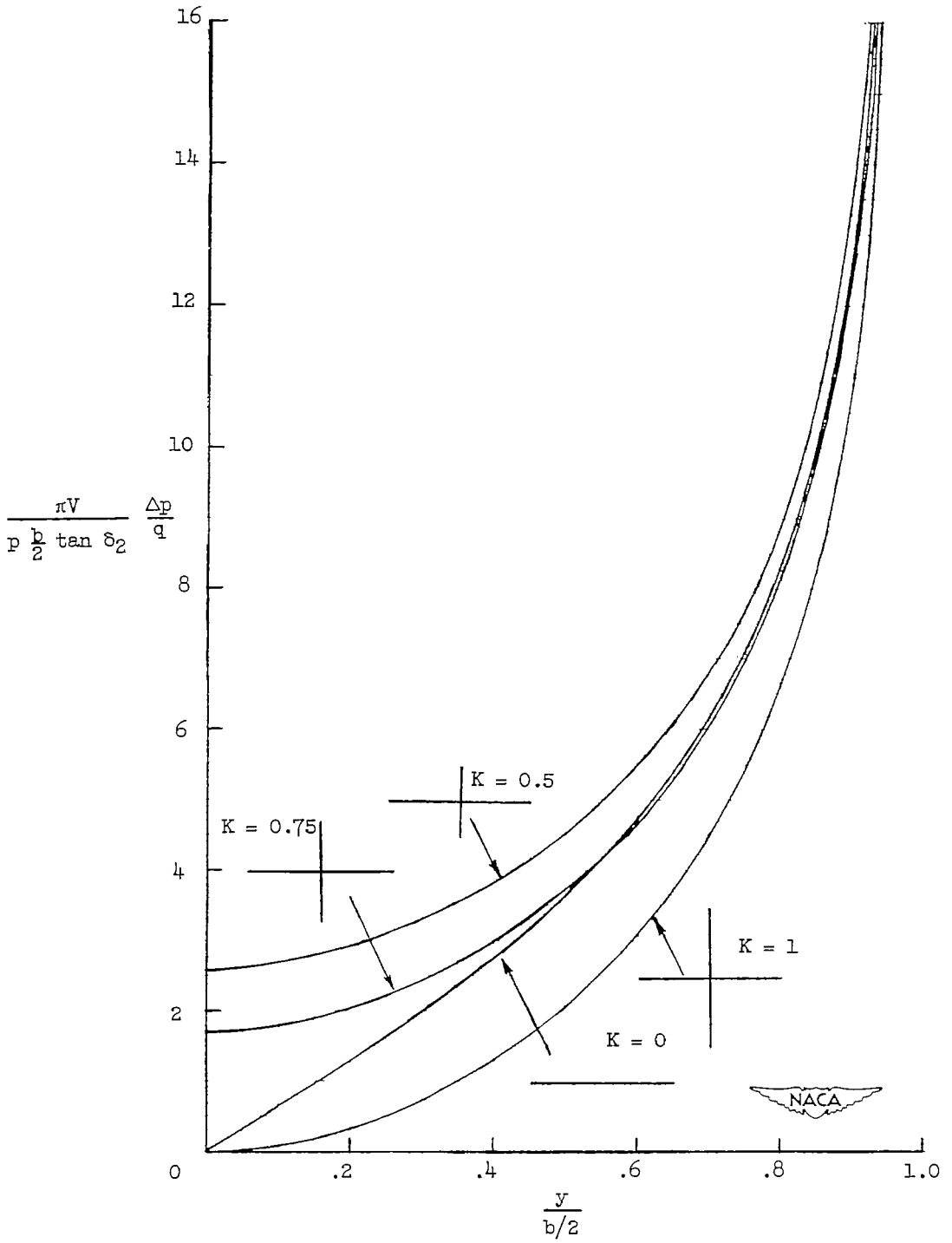

(a) Horizontal panels.

Figure 6.- Pressure distributions on the horizontal and vertical panels of four cruciform configurations with ratios of vertical-tail span to horizontal-tail span of 0, 0.5, 0.75, and 1.

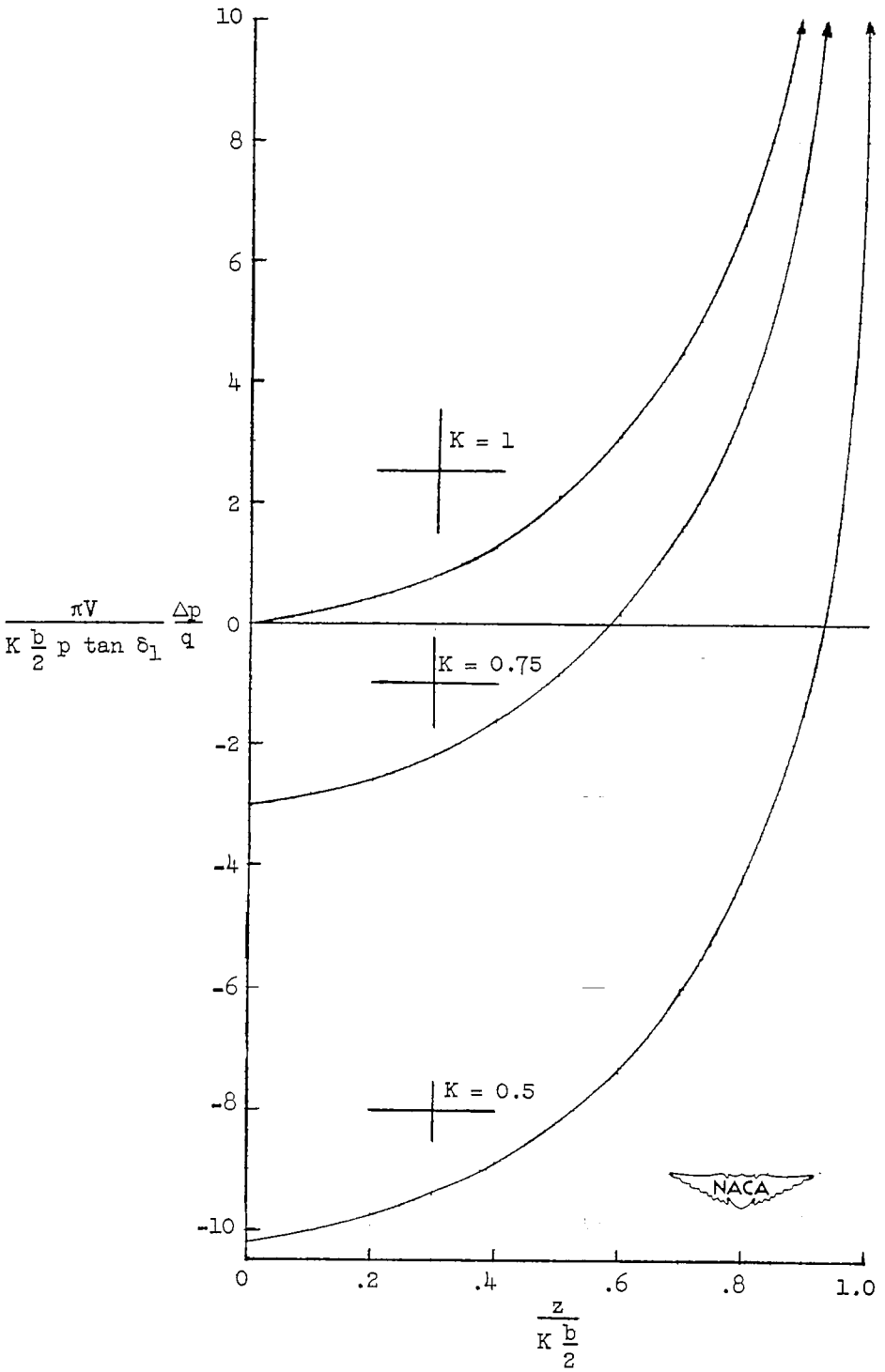

(b) Vertical panels.

Figure 6.- Concluded.

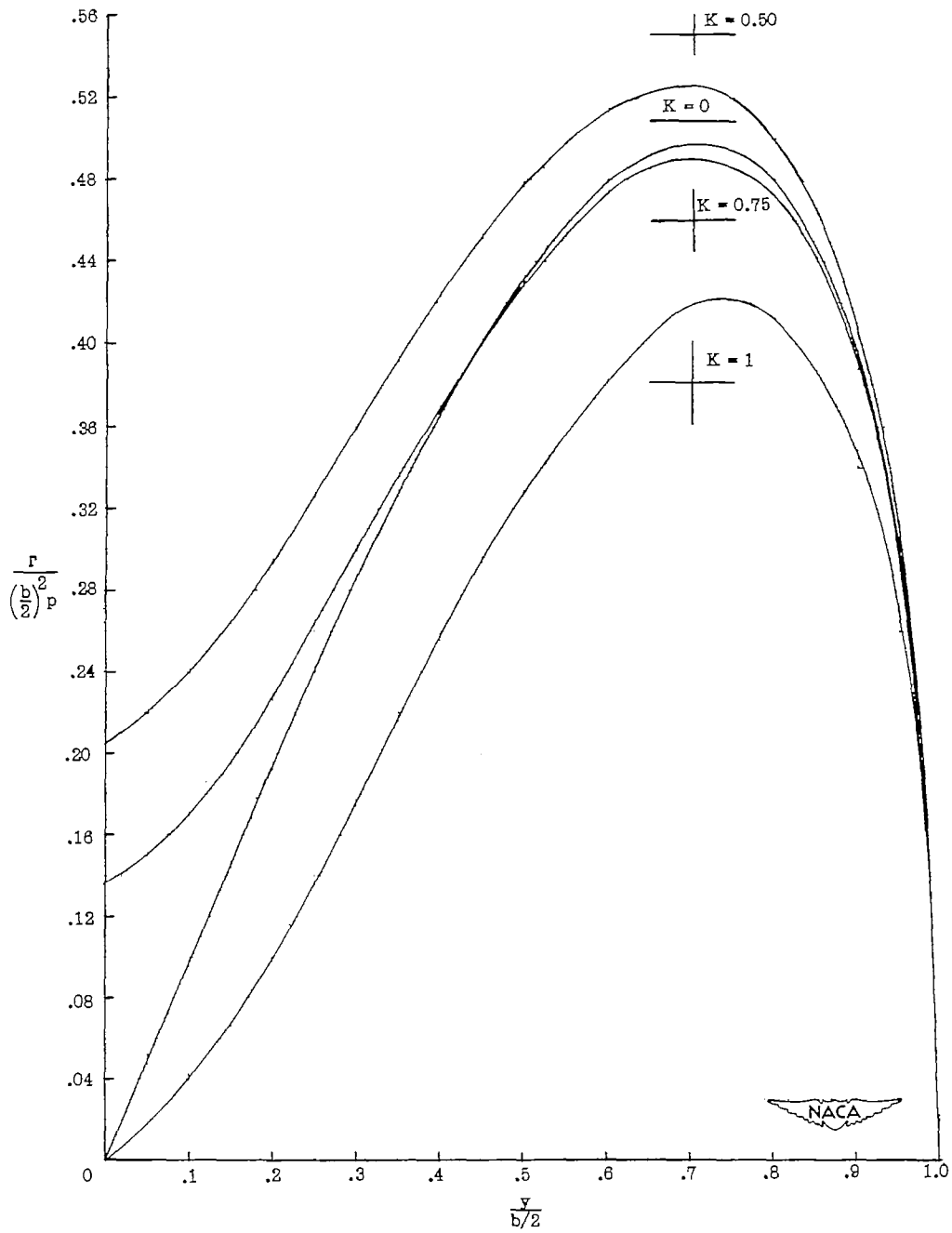

(a) Horizontal panels.

Figure 7.- The span loading in roll on the vertical and horizontal panels of four cruciform configurations with values of K of 0, 0.5, 0.75, and 1. Negative loading indicates damping forces directed in negative y-direction on upper vertical panel and in the positive y-direction on lower vertical panel.

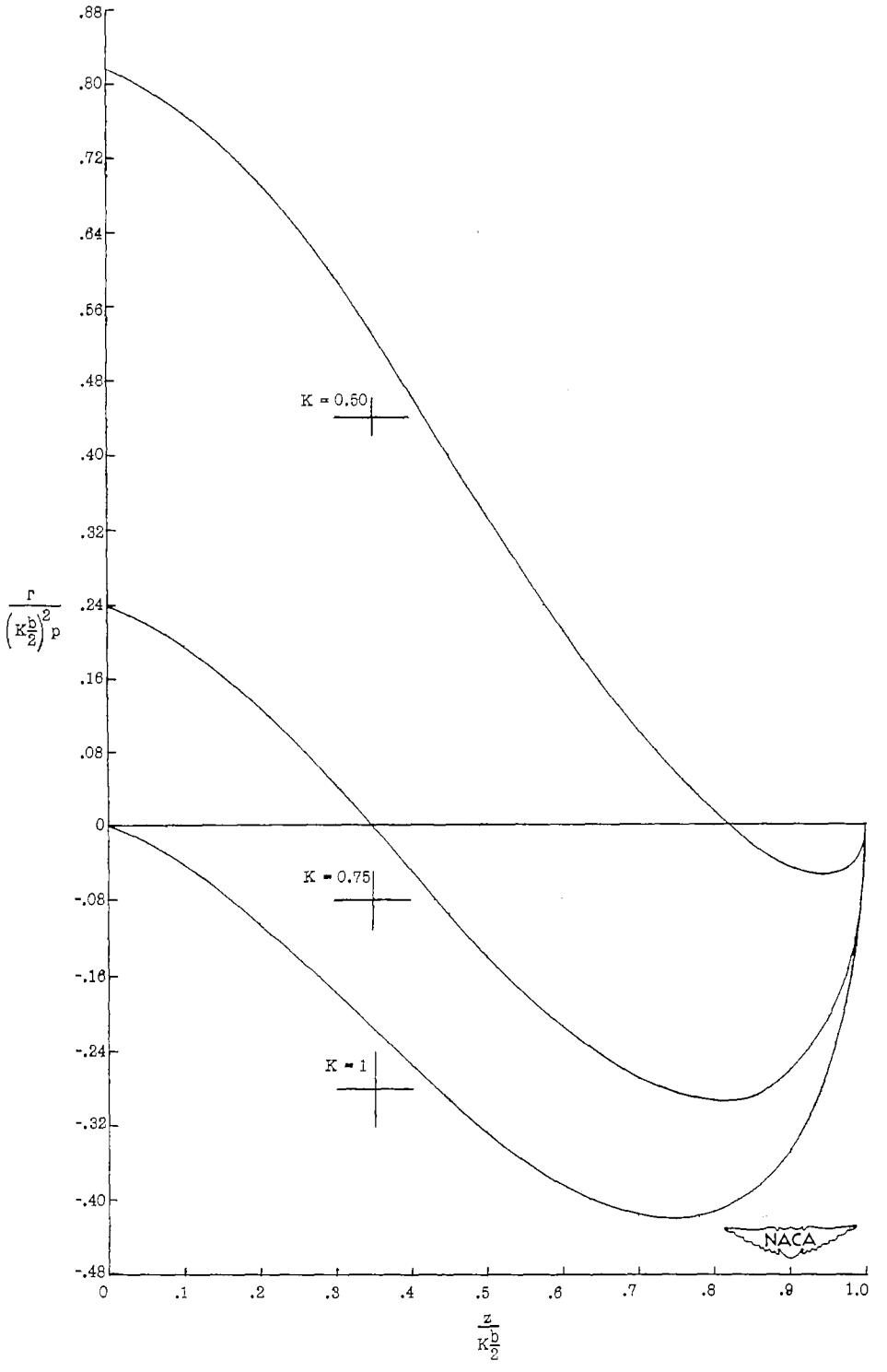

(b) Vertical panels.

Figure 7.- Concluded.

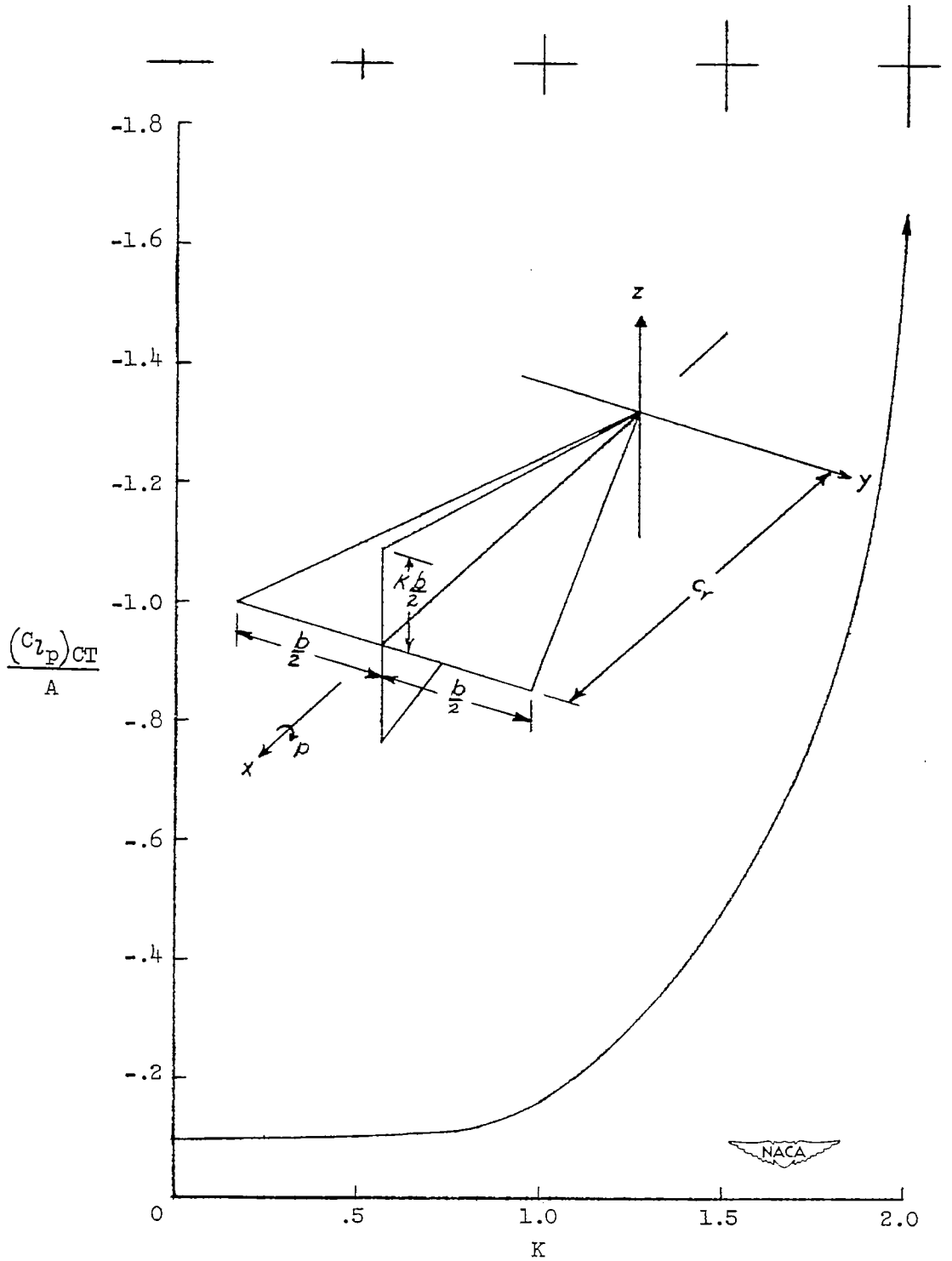

Figure 8.- The effect on the damping in roll of a slender cruciform tail of varying the ratio of the spans of the two mutually bisecting perpendicular wings.

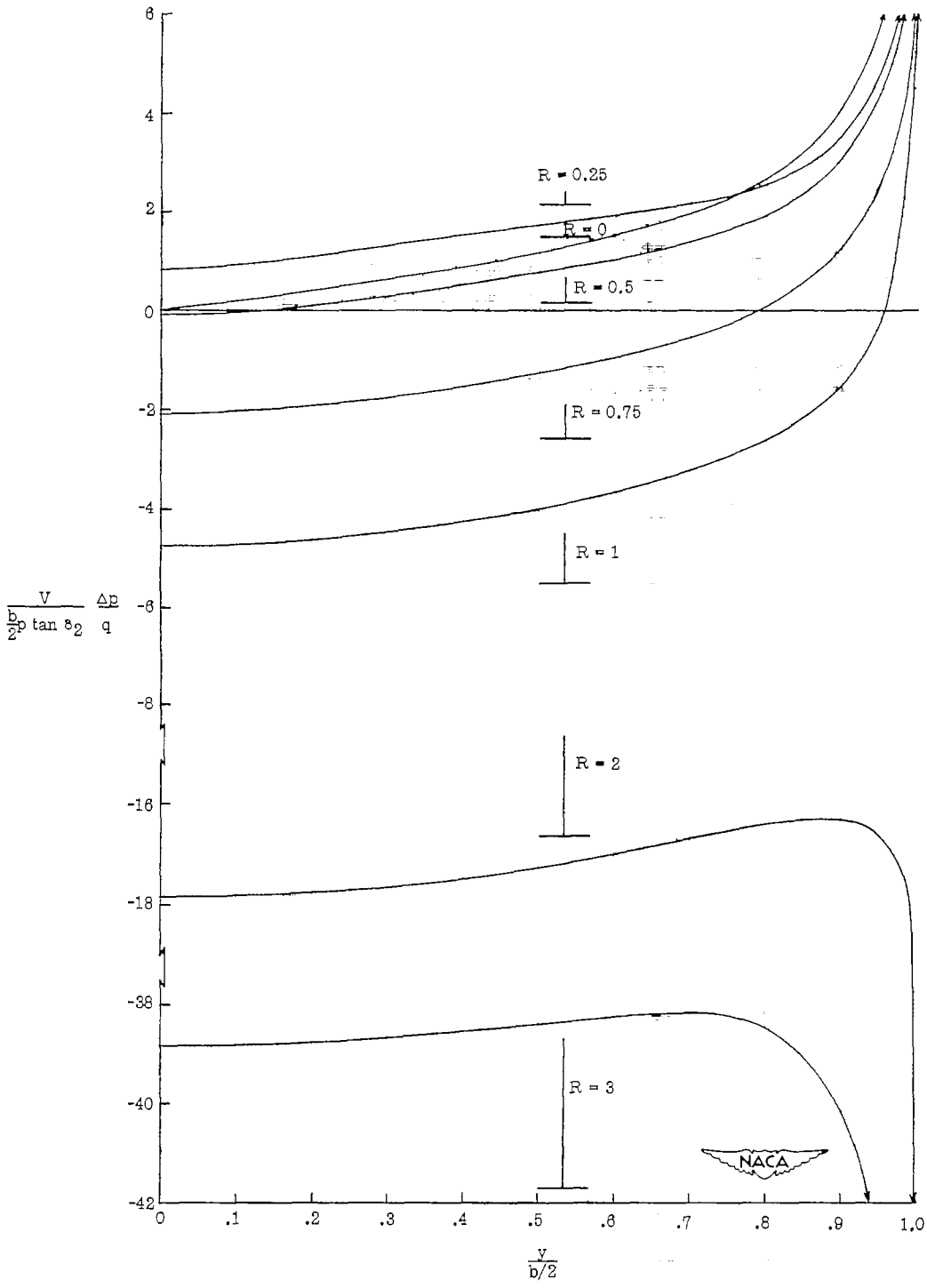

(a) Horizontal panels.

Figure 9.- Pressure distributions on the vertical and horizontal panels of a series of inverted T-tails.

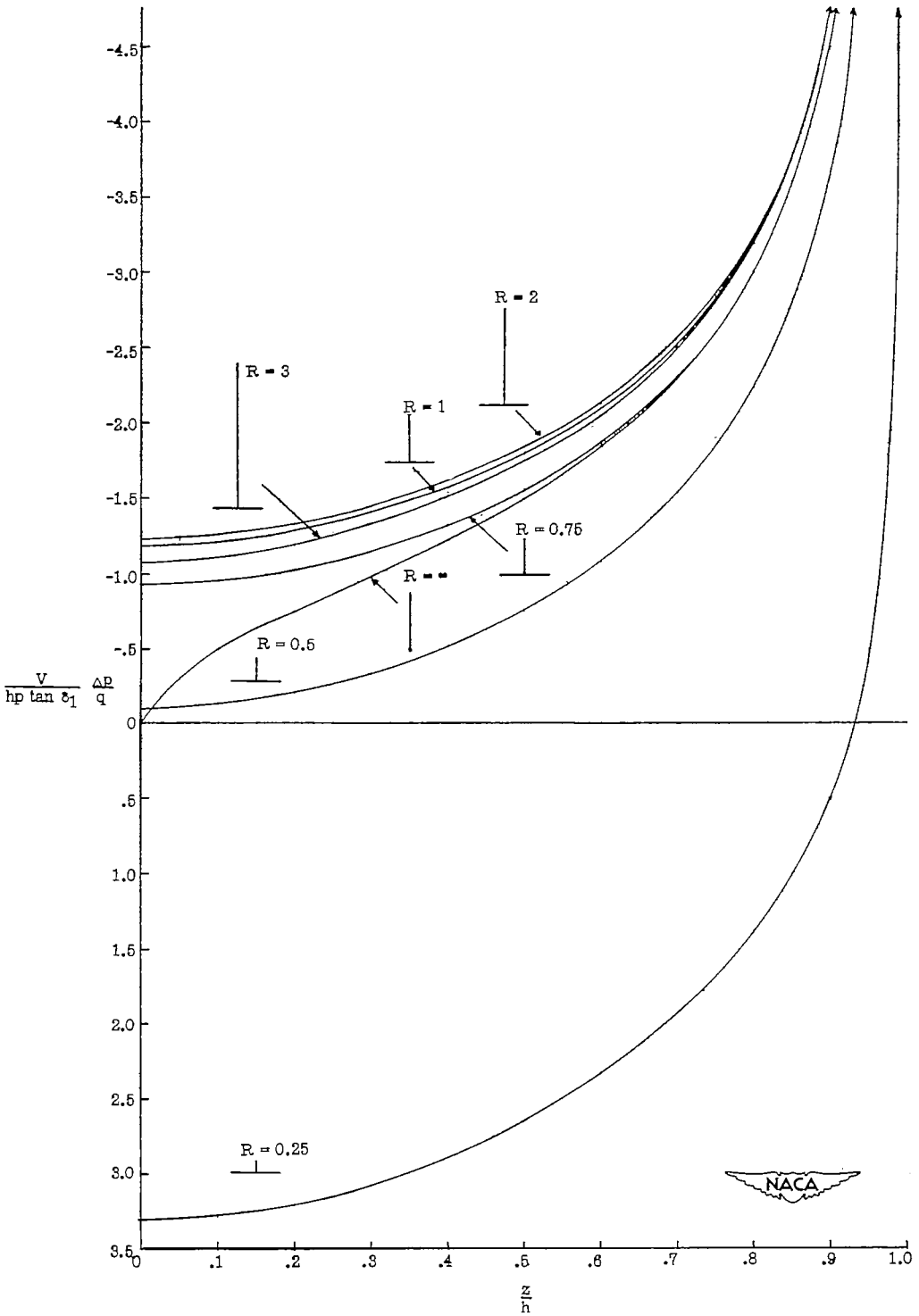

(b) Vertical panels.

Figure 9.- Concluded.

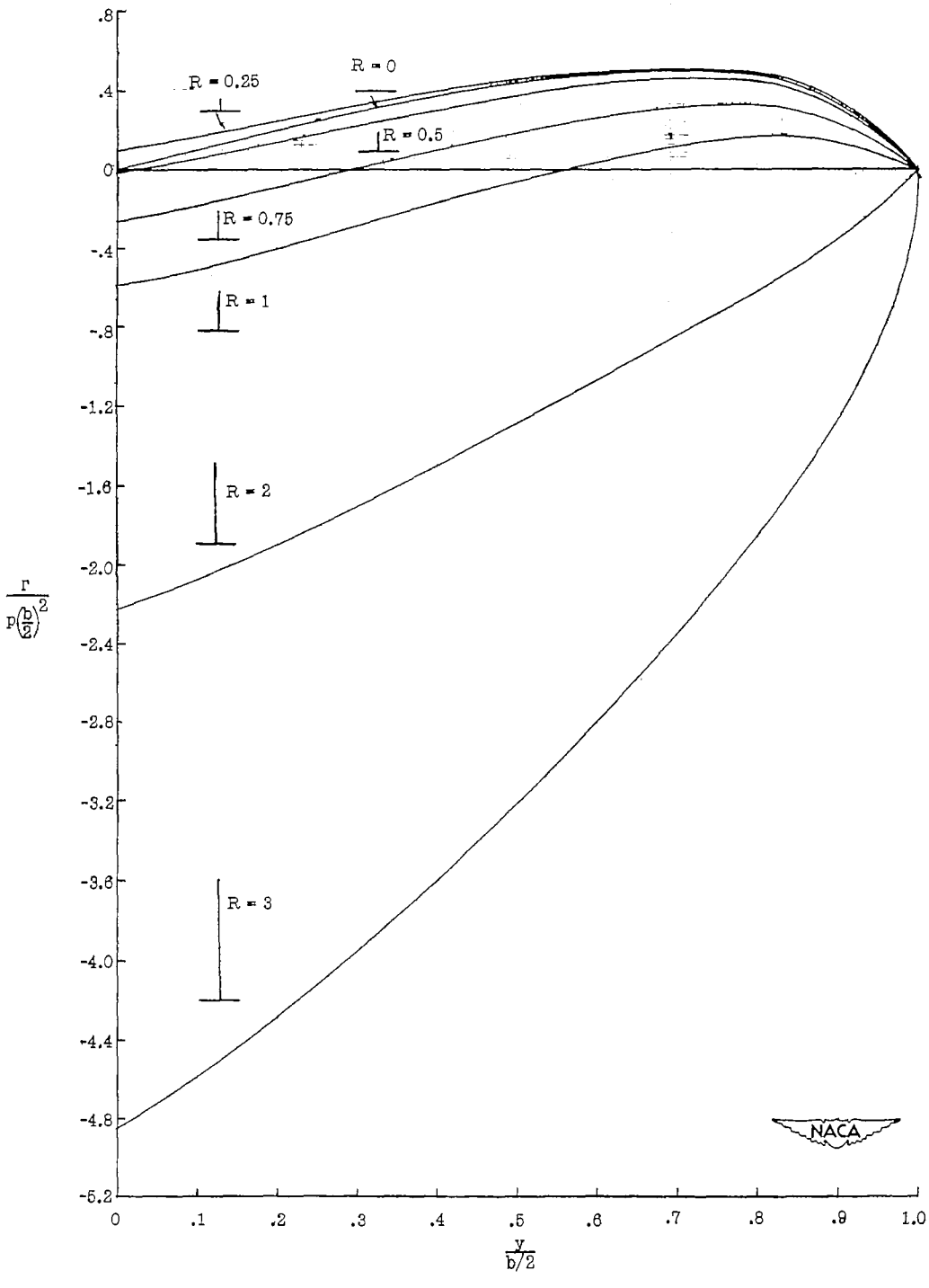

(a) Horizontal panels.

Figure 10.- The span loadings in roll on the vertical panel and horizontal tail of a series of inverted T-tails.

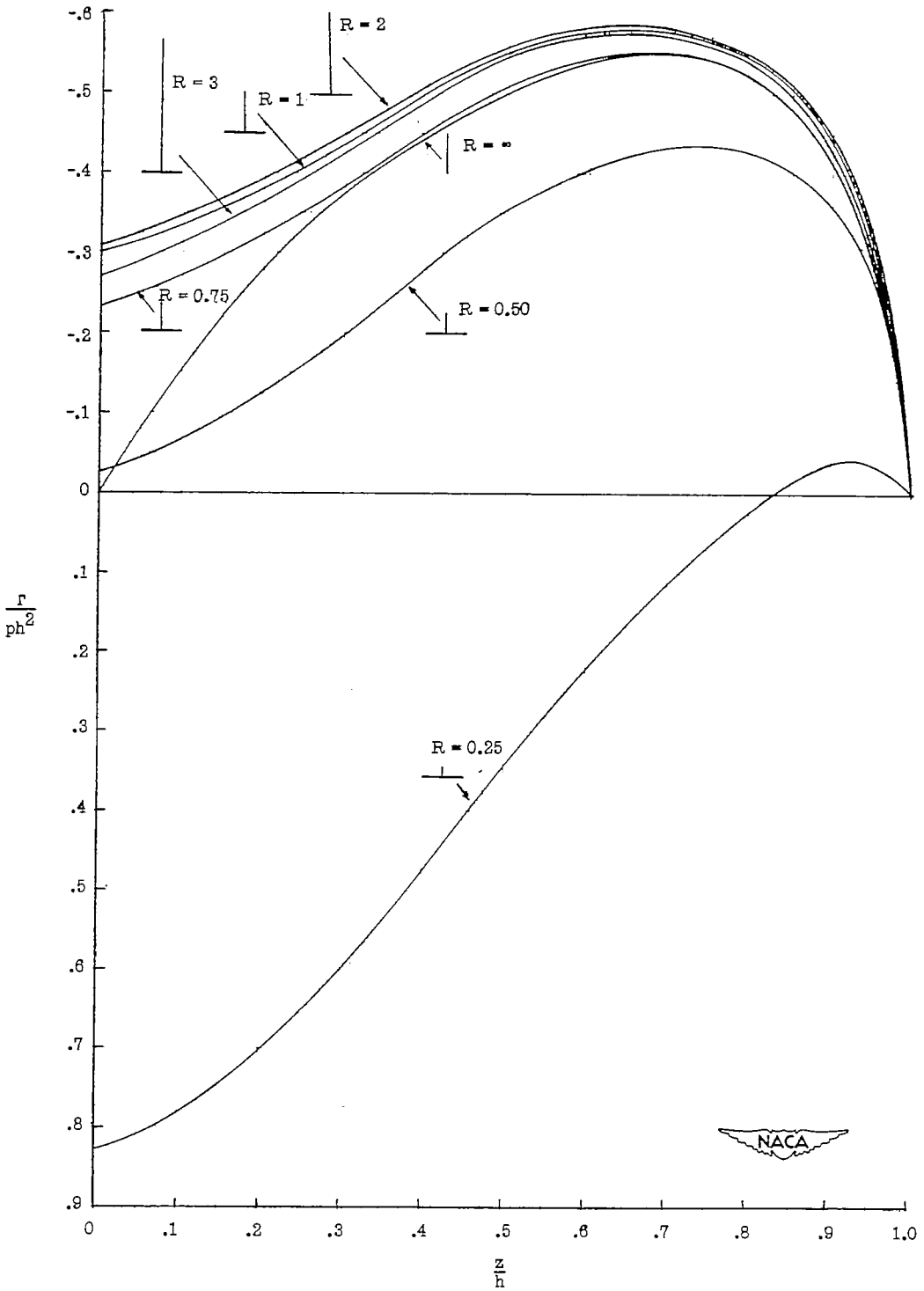

(b) Vertical panels.

Figure 10.- Concluded.

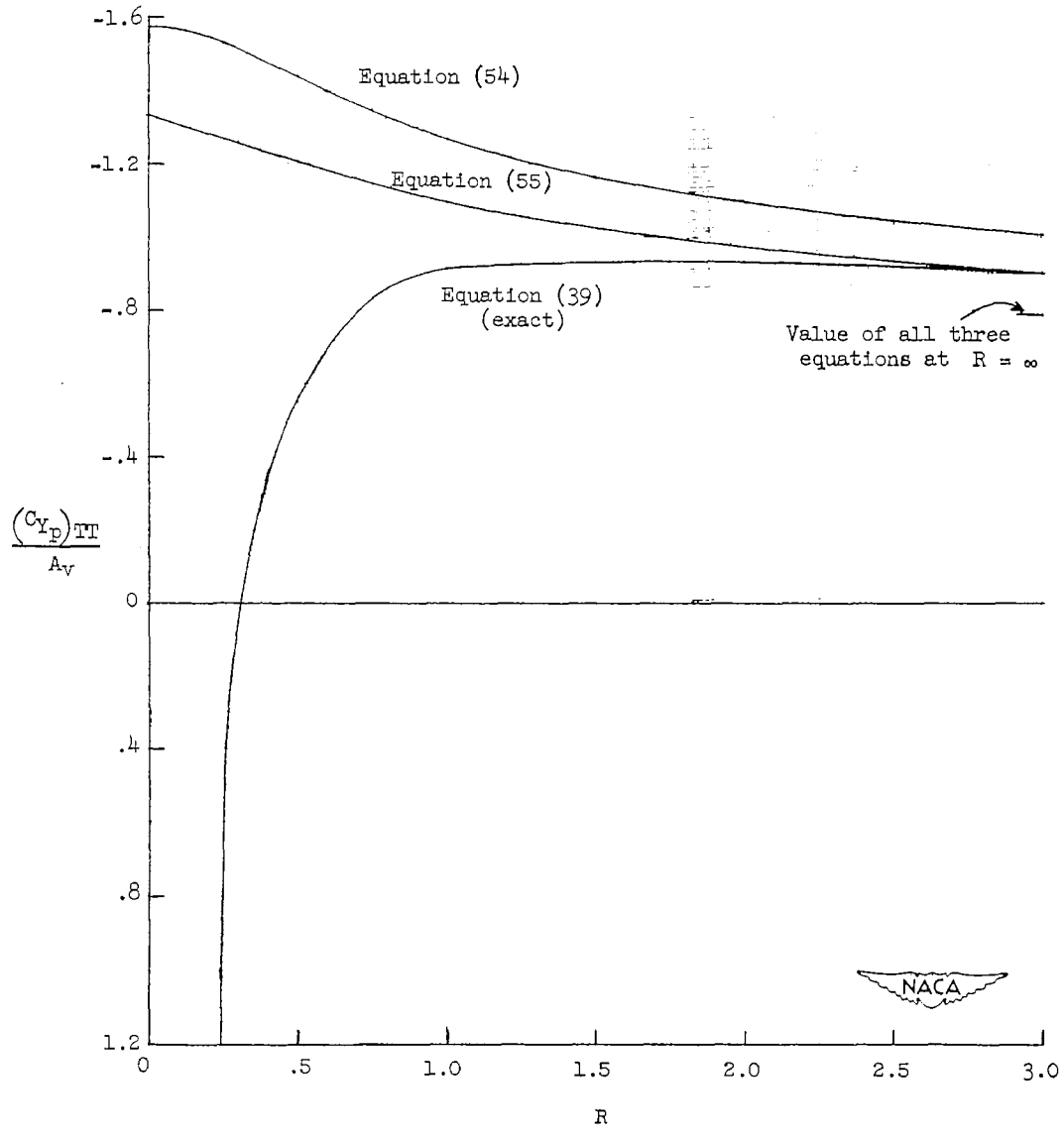

Figure 11.- The variation of the stability-derivative parameter $\frac{(C_{Y_p})_{TT}}{A_V}$ with R for a rolling inverted T-tail.

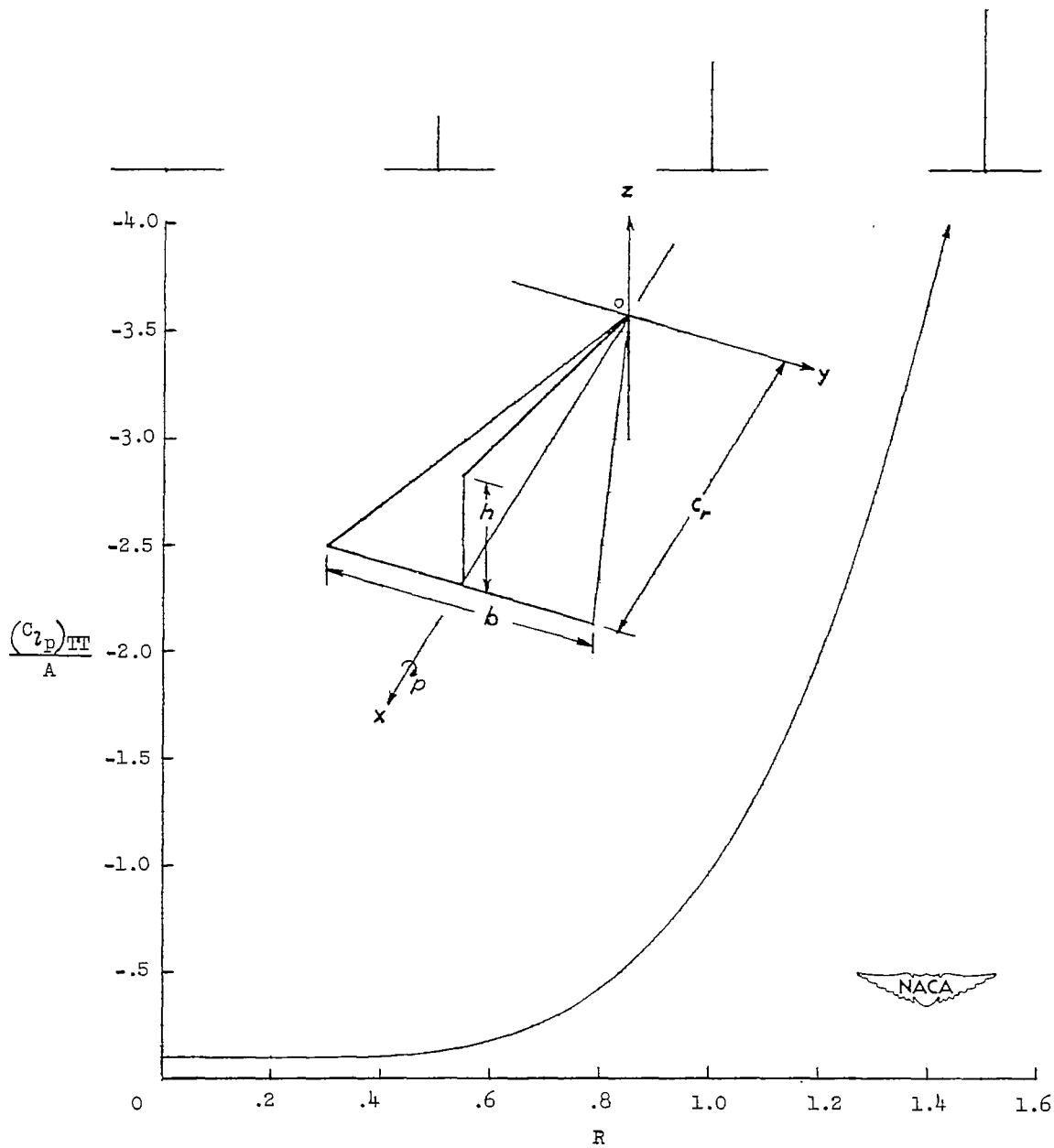

Figure 12.- Effect on damping in roll of adding a vertical panel to a slender triangular tail.

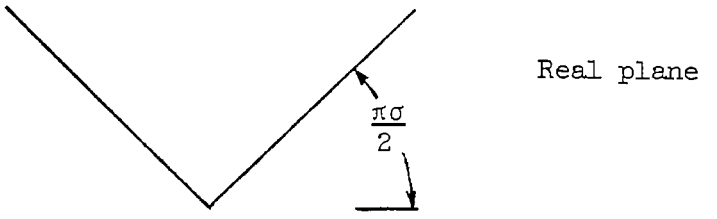

(a) Cross section of the V-tail in the physical plane.

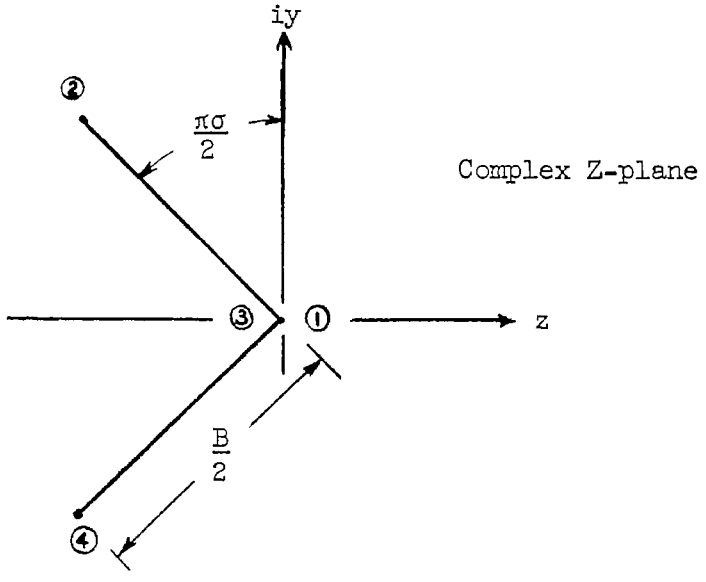

(b) V-tail oriented for two-dimensional analysis.

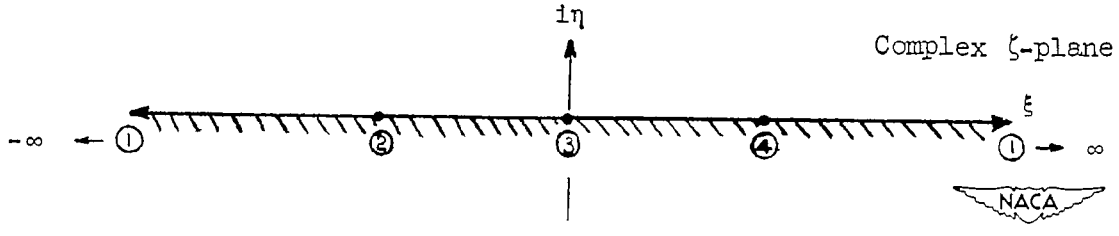

(c) Points in the ζ-plane corresponding to the vertices in the Z-plane.

Figure 13.- Physical and transformed planes used in analysis of rolling V-tail.

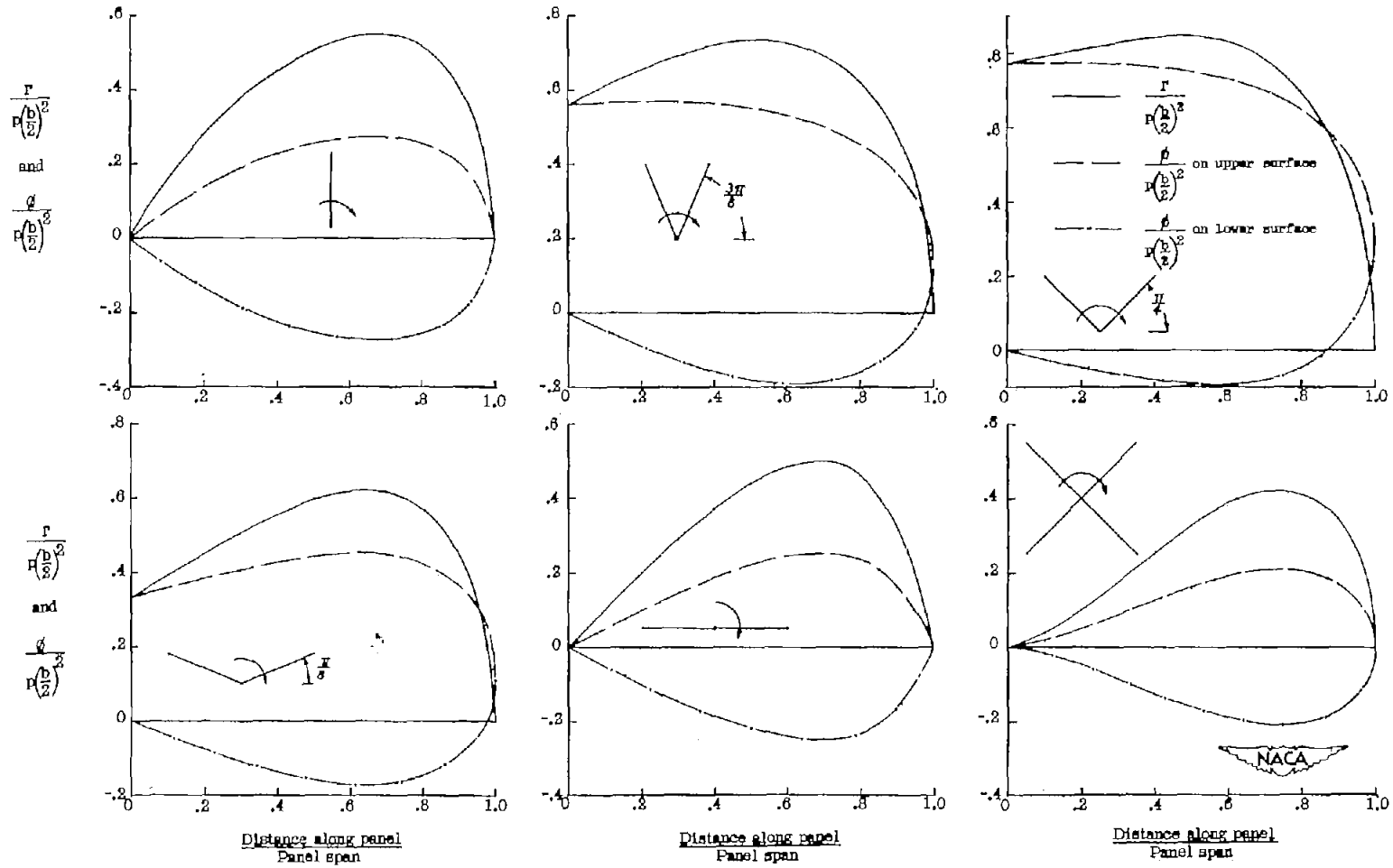

Figure 14.- The span load distributions and trailing-edge potentials on the right-hand panel of a series of V-tails in steady rolling. The span loading on a panel of an equi-panel-span cruciform is included for comparative purposes.

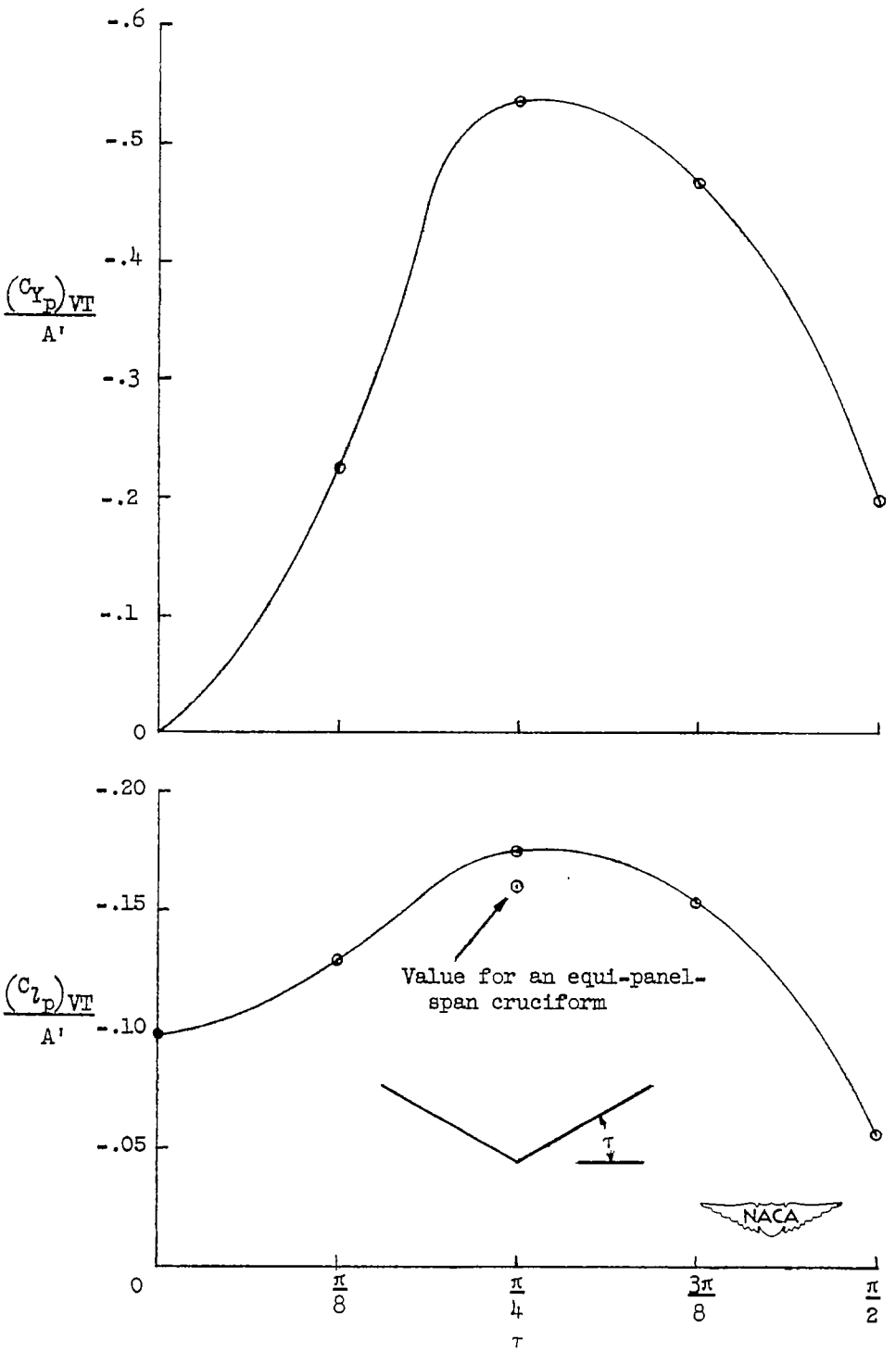

Figure 15.- Variation of the stability derivatives $\left(C_{Y_p}\right)_{VT}$ and $\left(C_{l_p}\right)_{VT}$ with the dihedral angle τ for a series of V-tails. The circled points indicate theoretical values.

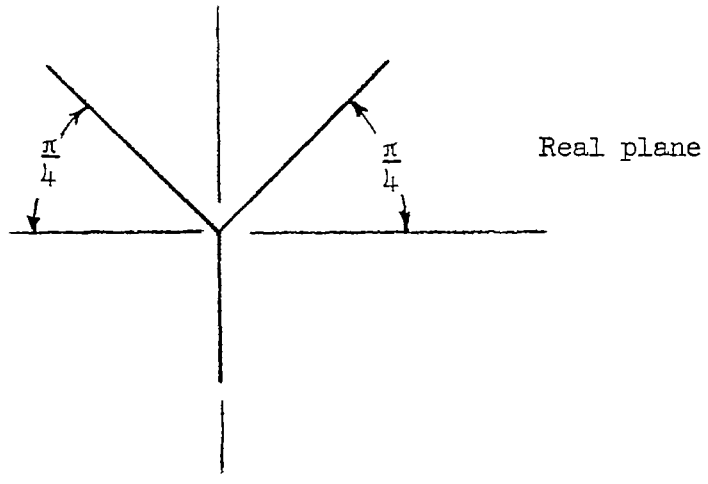

(a) Cross section of Y-tail in physical plane.

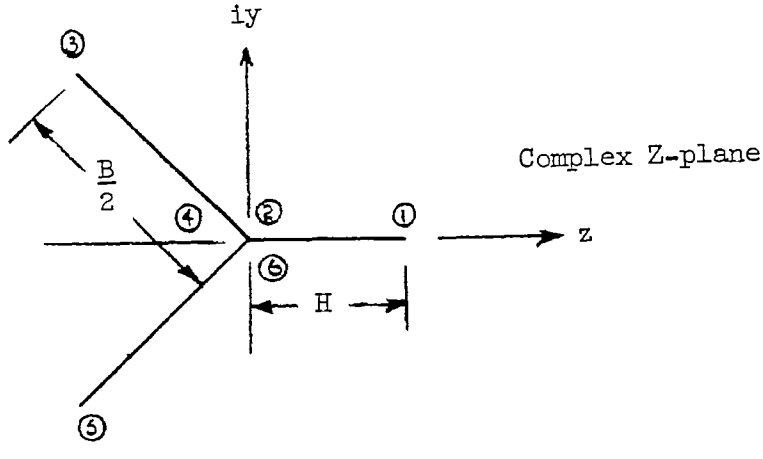

(b) Y-tail oriented for two-dimensional analysis.

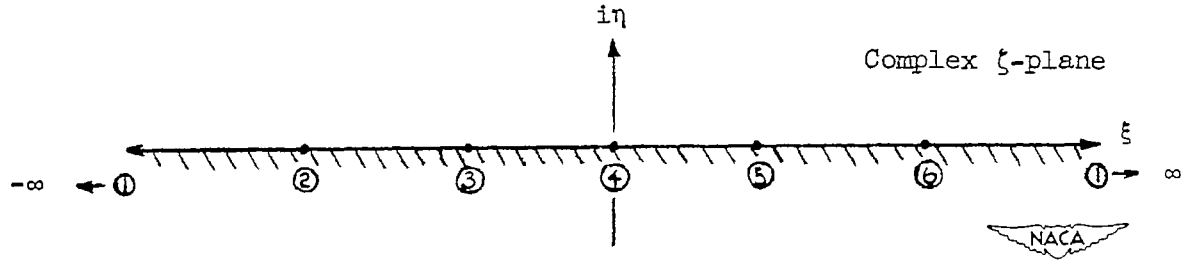

(c) Points in the ζ-plane corresponding to the vertices in the Z-plane.

Figure 16.- Physical and transformed planes used in analysis of rolling Y-tail.

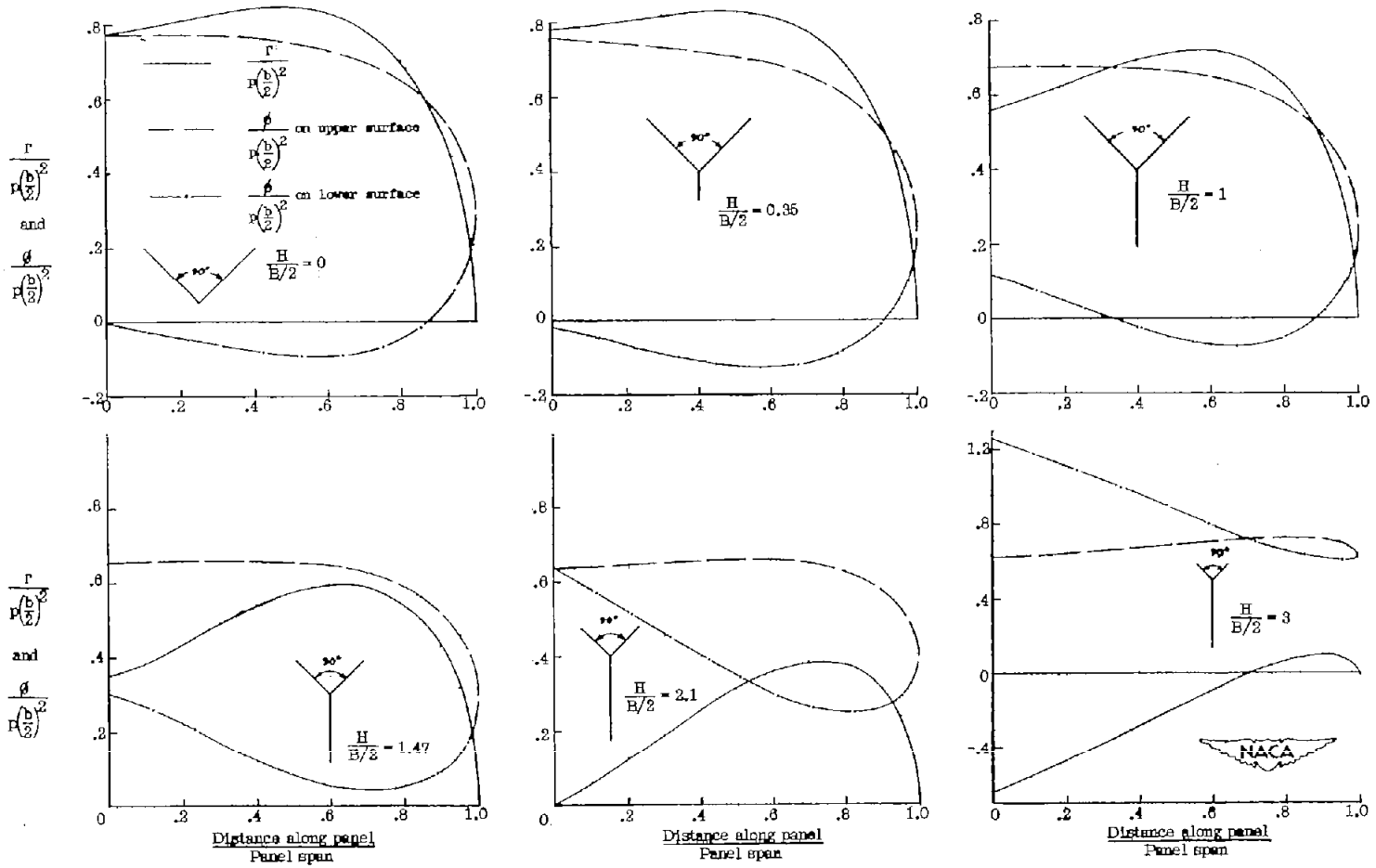

Figure 17.- The span load distributions and trailing-edge potentials on the inclined right-hand panels of a series of Y-tails in steady rolling. It should be noted that the small sketches on each graph are intended only to depict the ratio of the panel spans $\frac{H}{B/2}$.

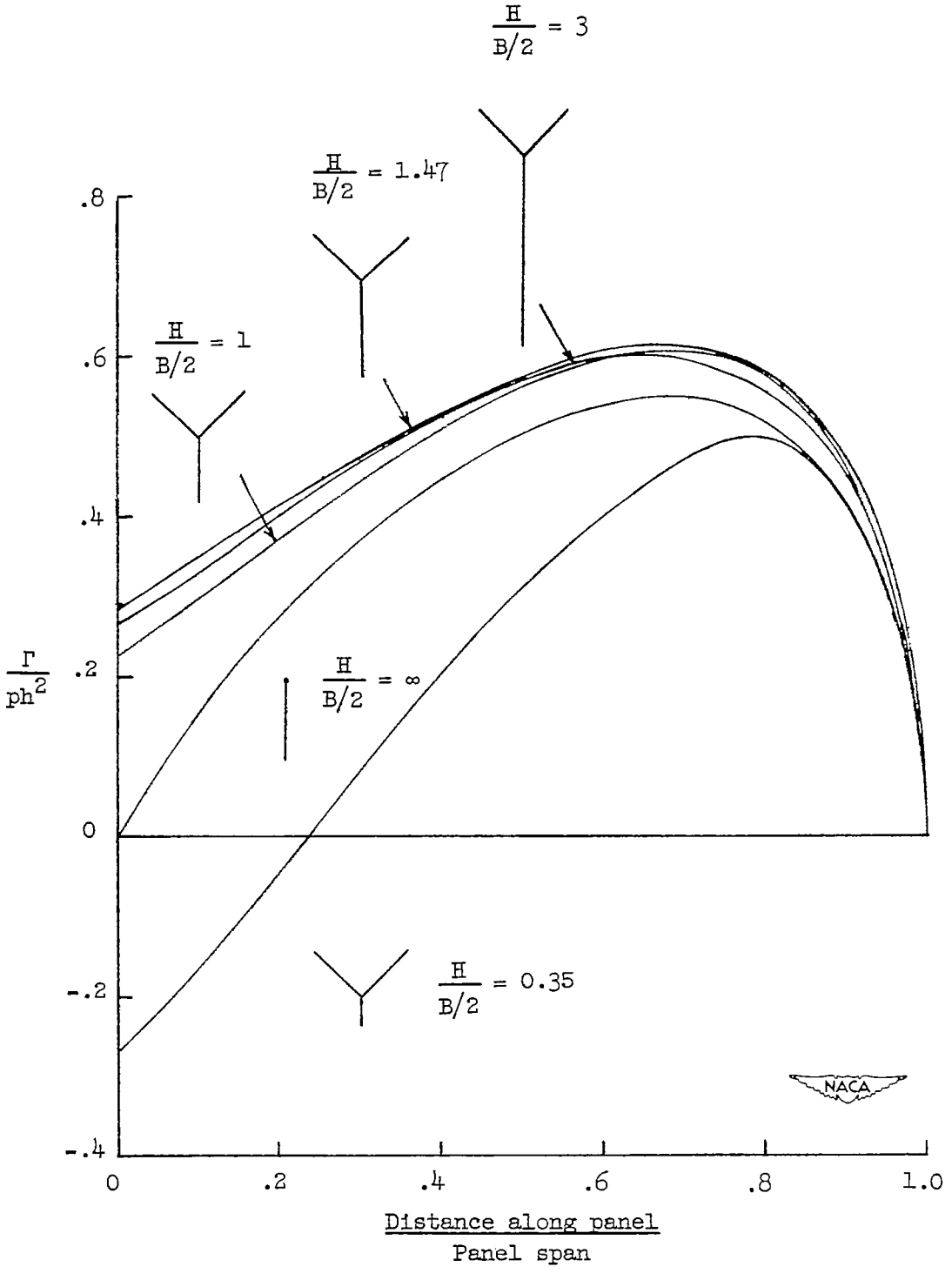

Figure 18.- The span loading in roll on the vertical panel of a series of Y-tails.

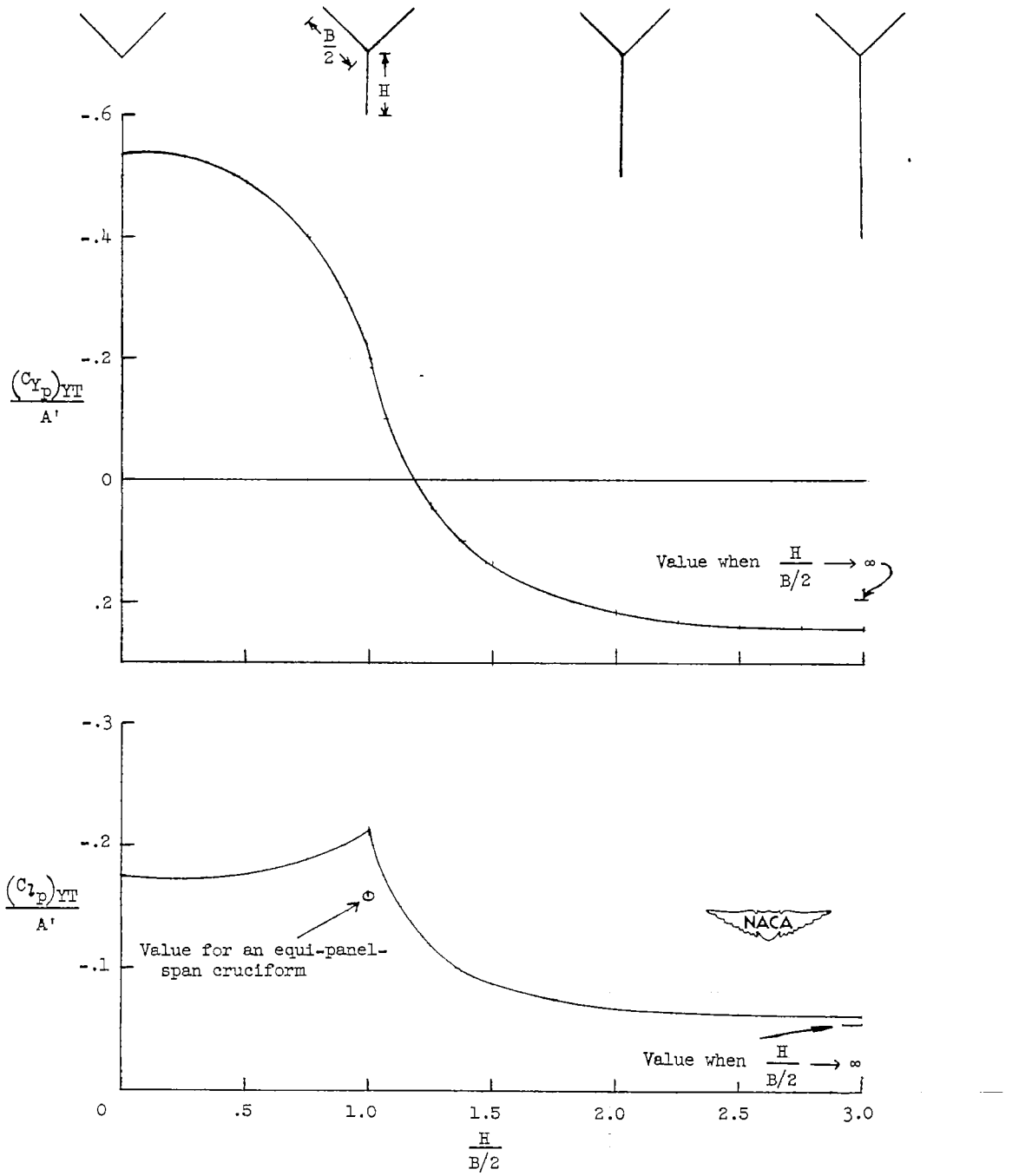

Figure 19.- The effect on the stability-derivative parameters $\left(C_{Y_p}\right)_{YT}$ and $\left(C_{l_p}\right)_{YT}$ of changing the span of the vertical panel on a slender Y-tail. The derivatives are nondimensionalized with respect to the diameter of the swept-out circle and twice the area of the largest panel.

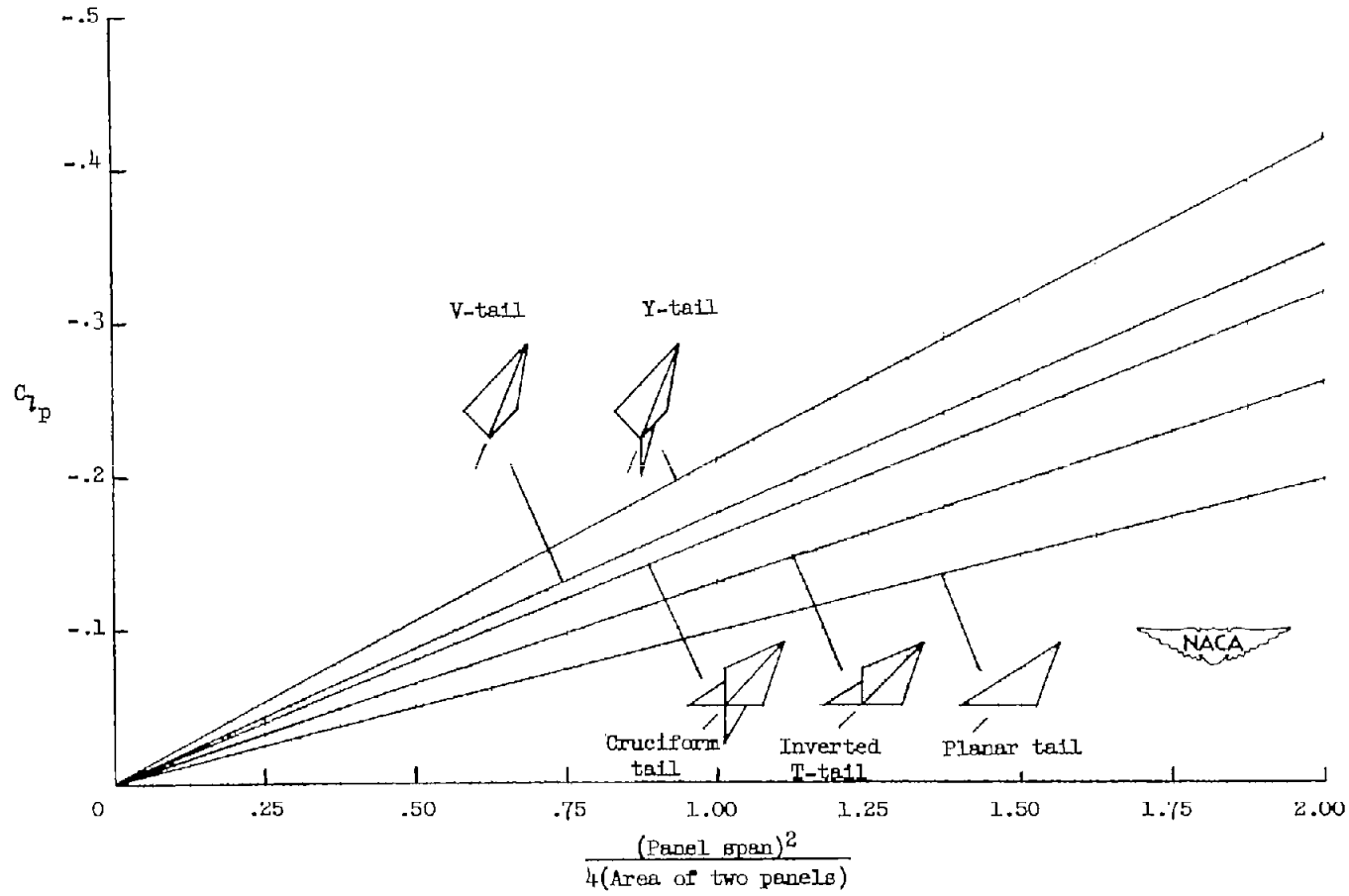

Figure 20.- Variation of C_{l_p} with aspect ratio for five slender configurations. All panels of the configurations are of equal span and area.

$$C_{l_p} = \frac{L'}{q(\text{Area of two panels})(\text{Twice panel span})\,\frac{p(\text{Panel span})}{V}}.$$

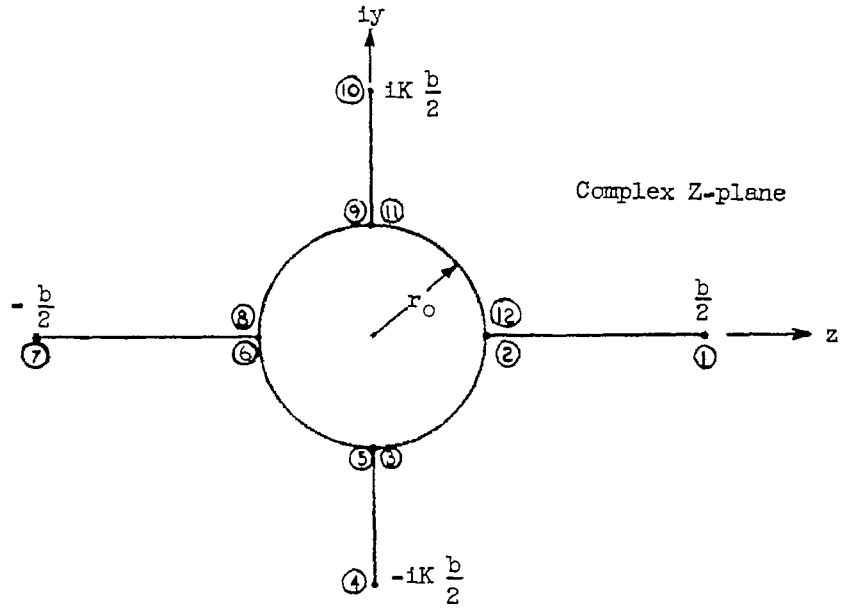

(a) Crossflow plane of cruciform-tail—body combination oriented for two-dimensional analysis.

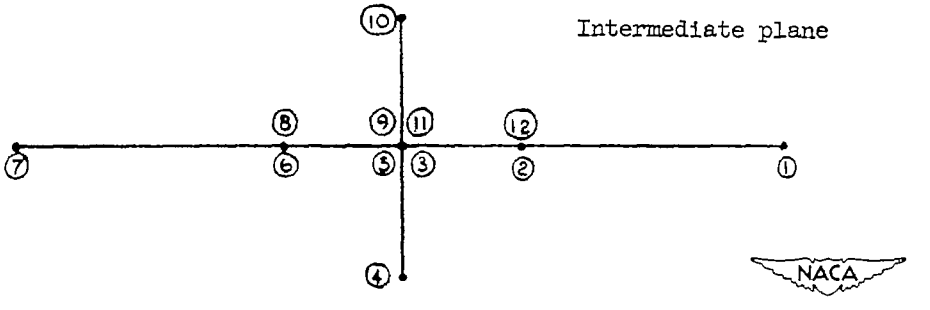

(b) Cruciform-tail—body combination transformed by Joukowski transformation.

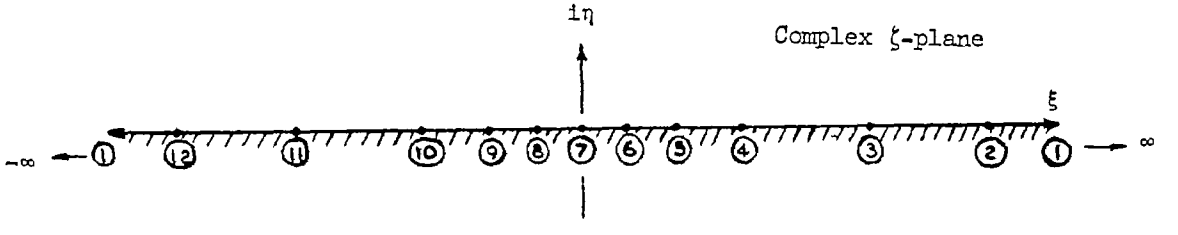

(c) Points in the ζ-plane corresponding to the vertices in the Z-plane.

Figure 21.- Physical and transformed planes used in analysis of rolling tail-body combination.

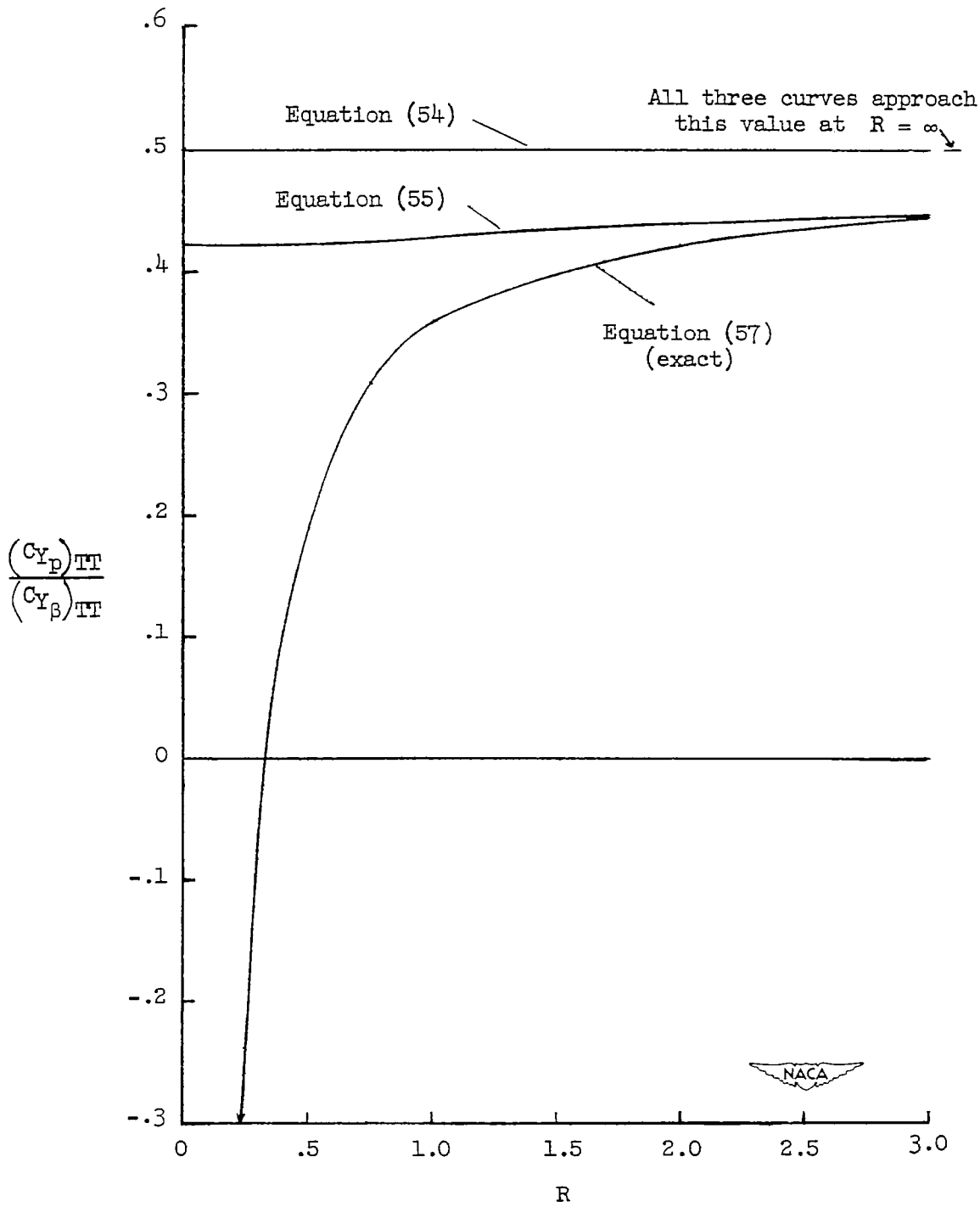

Figure 22.- The variation of the ratio $\left(C_{Y_p}\right)_{TT}/\left(C_{Y_\beta}\right)_{TT}$ with R for the inverted T-tail as determined by exact and approximate methods. At $R = \infty$ all equations give ratio equal to 0.5.

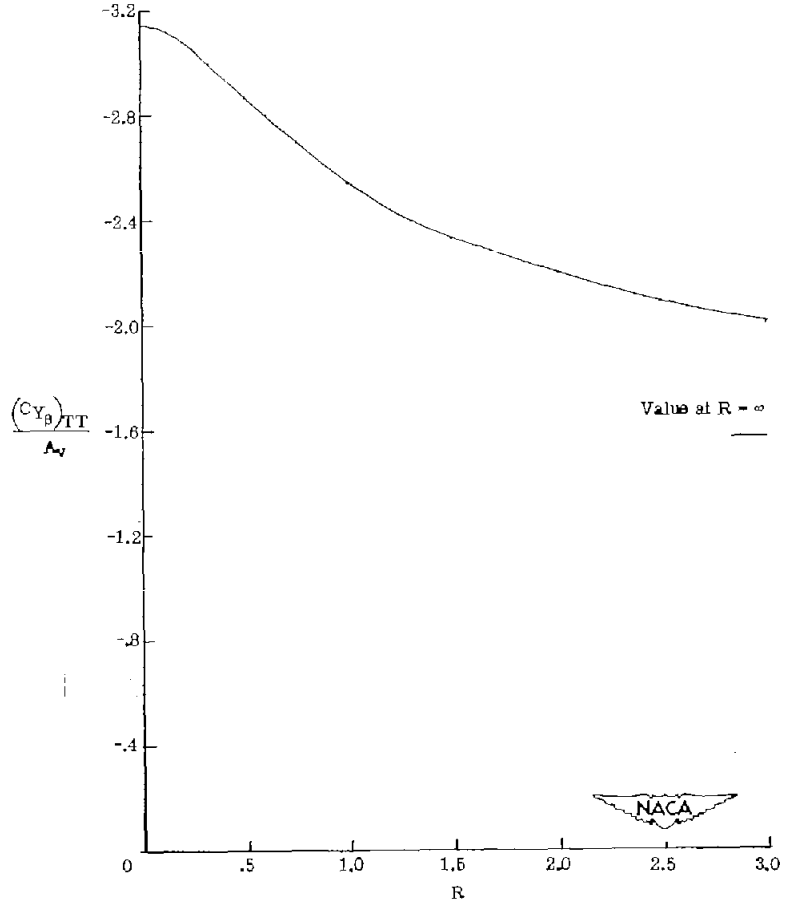

Figure 23.- The variation of $(C_{Y_\beta})_{TT}$ with R for a sideslipping inverted T-tail.

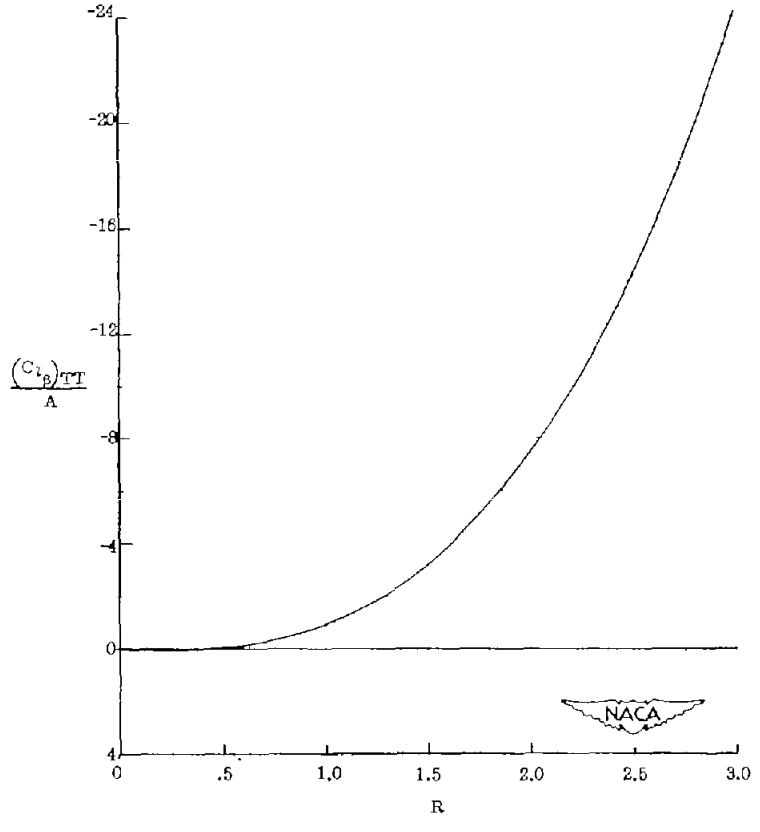

Figure 24.- The variation of $(C_{l_\beta})_{TT}$ with R for a sideslipping inverted T-tail.

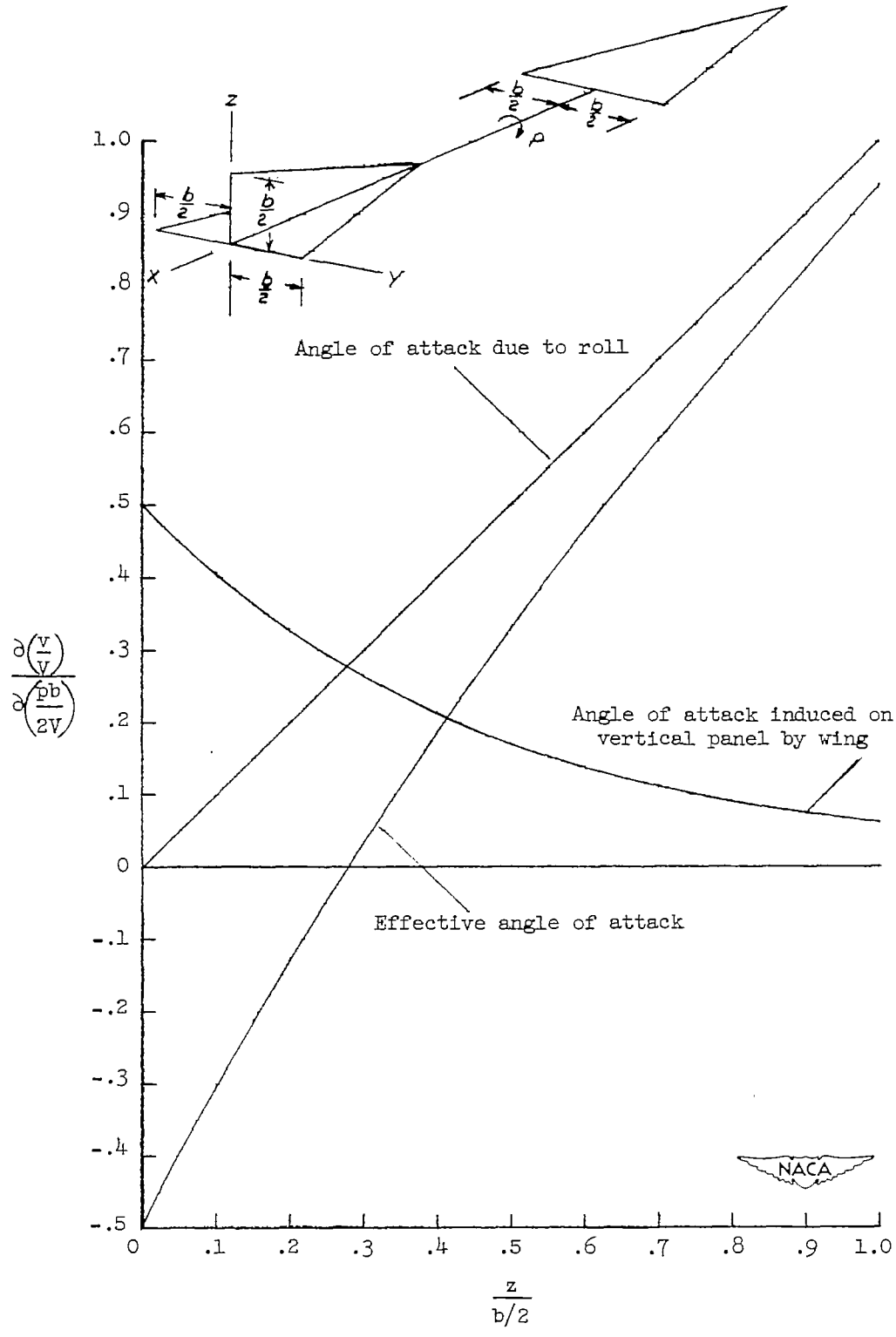

Figure 25.- The effect of sidewash from a slender rolling wing on the angle-of-attack distribution along the vertical panel of a T-tail.